Ore Geology Reviews 159 (2023) 105561

Contents lists available at ScienceDirect

Ore Geology Reviews

journal homepage: www.elsevier.com/locate/oregeorev

Review

Evolutionary paths for the formation of different types of fluid inclusions in the H_2O-NaCl system

Wei Mao [a,*], Hong Zhong [a,b], Thomas Ulrich [c]

[a] State Key Laboratory of Ore Deposit Geochemistry, Institute of Geochemistry, Chinese Academy of Sciences, Guiyang 550081, China
[b] University of Chinese Academy of Sciences, Beijing 100049, China
[c] Department for Geoscience, Aarhus University, Aarhus 8000, Denmark

ARTICLE INFO

Keywords:
Fluid inclusion
Numerical calculation
Phase ratios
Evolutionary path
Contour figures

ABSTRACT

Previous studies revealed very complicated phase ratios and microthermometric behavior of fluid inclusions, which can be attributed to the various phase relations in the H_2O-NaCl system and different evolutionary paths after their entrapment at different conditions. This numerical calculation work aims at presenting a comprehensive illustration of fluid inclusion formation in the H_2O-NaCl system and facilitating the interpretation of microthermometric data. We firstly illustrate a series of contours figures in the pressure–temperature projection for fluid salinities at 0.1, 1, 10, 30, 50, and 70 wt% NaCl, for the bubble curve and the dew curve, and for the halite liquidus of the H_2O-NaCl system to demonstrate the changes of salinities and densities that lead to the variations of room-temperature phase ratios of fluid inclusions. Then we comprehensively construct the evolutionary paths of fluids trapped at variable conditions. Isochores of the entrapped halite-undersaturated fluids may intersect the vapor + liquid surface of the H_2O-NaCl system on the dew curve, the bubble curve, or the locus on the critical curve, or intersect the bubble curve of the vapor + halite region. Isochores of the entrapped halite-saturated fluids may intersect the bubble curve of the vapor + liquid surface at elevated temperature, the dew curve of the vapor + liquid surface, the halite liquidus, or their junction. After the intersections, the fluid inclusions evolve in the two-phase regions (vapor + liquid, liquid + halite, or vapor + halite), and the detailed evolution of fluid pressure, temperature, density, salinity, and phase ratios of the coexisting two phases are systematically discussed. Evolutionary paths of the halite-saturated fluids and the extremely low salinity fluids will eventually intersect the vapor + liquid + halite surface and then evolve to room temperature.

The evolutionary paths above define nine types of fluid inclusions with characteristic phase ratios and microthermometric behavior, making a necessary complement to previous studies for the understanding of fluid inclusion formation and interpretation of microthermometric data. For the first time, we present the evolutionary path for a halite-bearing fluid inclusion that experiences partial homogenization by halite dissolution and total homogenization by liquid disappearance. Underestimation of the homogenization temperature is inevitable for vapor-rich fluid inclusions formed in the vapor + halite region, therefore, such fluid inclusions, typically formed in very shallow porphyry systems, provide invalid temperature information for fluid evolution. The residual vapor phase at halite dissolution for halite-bearing fluid inclusions may lead to an over-estimation of the bulk fluid salinity by over 3 % at elevated temperature conditions. The contour figures can facilitate the understanding of post-entrapment modifications of fluid inclusions which alters fluid inclusion phase ratios and homogenization behavior.

1. Introduction

Fluid inclusion studies of magmatic-hydrothermal deposits have revealed the complexity of fluid inclusion phase variations and microthermometry behavior (Roedder, 1971; Heinrich et al., 1999; Becker et al., 2008; Bodnar et al., 2014). For example, the vapor phase proportion of fluid inclusions at room-temperature ranges from <5 vol% up to 100 vol%. Similarly, a variety of daughter minerals including halite, sylvite, calcite, and opaque minerals have been documented in many deposits. The fluid salinity in different deposits ranges from <1 wt%

* Corresponding author.
E-mail address: maowei@mail.gyig.ac.cn (W. Mao).

https://doi.org/10.1016/j.oregeorev.2023.105561
Received 15 March 2023; Received in revised form 16 June 2023; Accepted 20 June 2023
Available online 24 June 2023

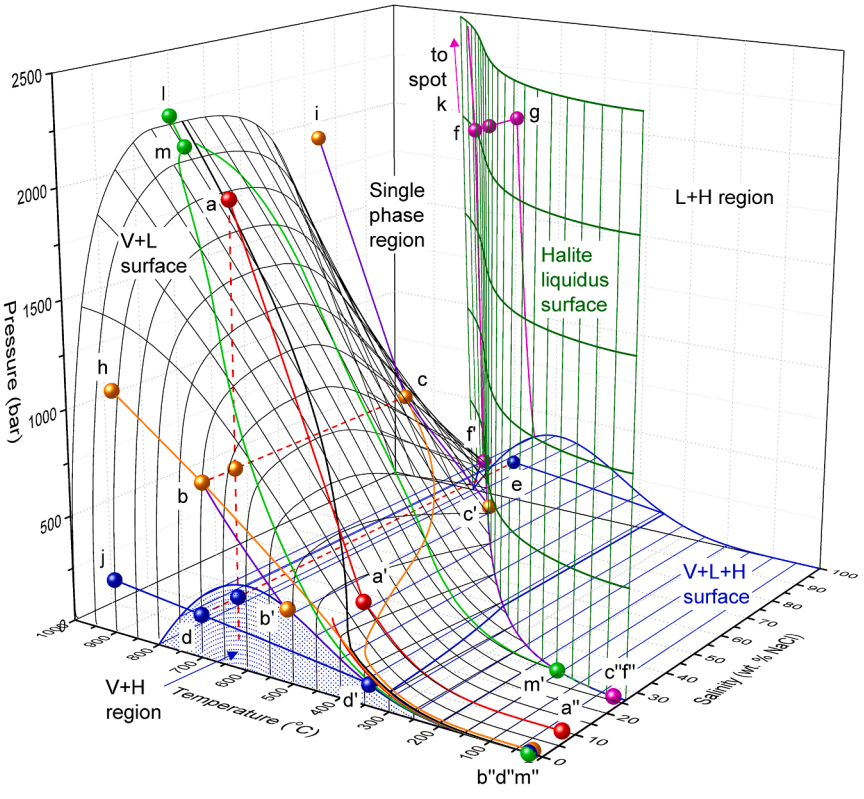

Fig. 1. Pressure–temperature-salinity diagram of the H_2O-NaCl system. Constructed with equations in Driesner and Heinrich (2007) and Driesner and Heinrich (2007). Point a, h, i, j, k, and l are in the single-phase region; points b, c and m are on the vapor + liquid coexistence surface; point d is on the bubble curve of the vapor + halite region; point f is on the halite liquidus; point e is pure halite at the same pressure–temperature condition to point d; point g is pure halite at the same pressure–temperature condition to point g. See Table 1 for detailed pressure–temperature-salinity conditions of each point. Evolutionary paths of trapped fluids under variable conditions are constructed. See text for detailed discussion. V-vapor, L-liquid, H-halite.

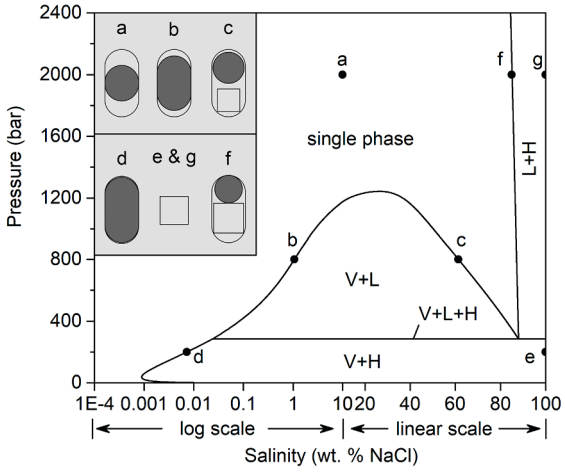

Fig. 2. The 700 ℃ isotherm section of the H_2O-NaCl system. Constructed with equations in Driesner and Heinrich (2007) and Driesner and Heinrich (2007). Labels a to g are consistent with those in Fig. 1. The inset shows the appearances of fluid inclusions trapped at the labeled points. Salinity below 10 wt% NaCl is plotted as log10 (wt.% NaCl) for better illustration. V-vapor, L-liquid, H-halite.

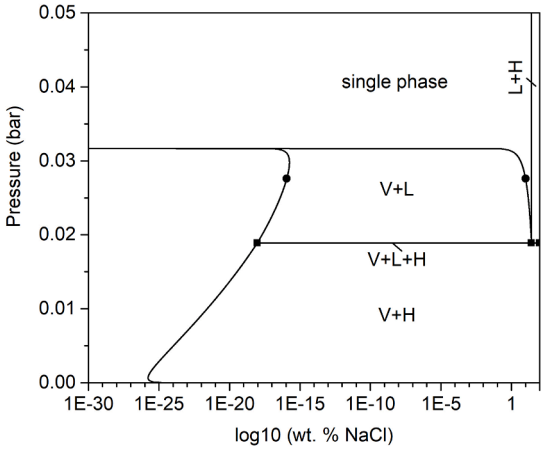

Fig. 3. The 25 °C isotherm of the H_2O-NaCl system. Constructed with equations from Driesner and Heinrich (2007). The black points demonstrate the conditions of the vapor and liquid phases of a V + L fluid inclusion trapping a 10 wt% NaCl solution. The black squares demonstrate the conditions of the vapor, liquid, and halite of a V + L + H fluid inclusion trapping the halite-saturated solution. Salinity is plotted as log10 (wt. % NaCl) for clearer illustration. V-vapor, L-liquid, H-halite.

NaCl equiv. up to >70 wt% NaCl equiv. (Bodnar et al., 2014). The parental magmatic fluid originating from the magma chamber is inferred to be in the range of 2 to 15 wt% NaCl equiv. (Cline and Bodnar, 1991; Audétat et al., 2008; Rusk et al., 2008; Audétat and Li, 2017; Mao et al., 2017). These are some of the general characteristics of magmatic-hydrothermal fluids, but their wide range of homogenization behaviors (homogenizing to liquid, to vapor, by halite melting, and by disappearance of the meniscus) can make it complicated for the interpretation of pressure–temperature conditions of the fluid evolution (Ermakov, 1965; Knight and Bodnar, 1989; Bodnar, 1994; Audétat et al., 1998; Bodnar, 2003; Becker et al., 2008; Bodnar et al., 2014; Lecumberri-Sanchez et al., 2015a; Lecumberri-Sanchez et al., 2015b; Lecumberri-

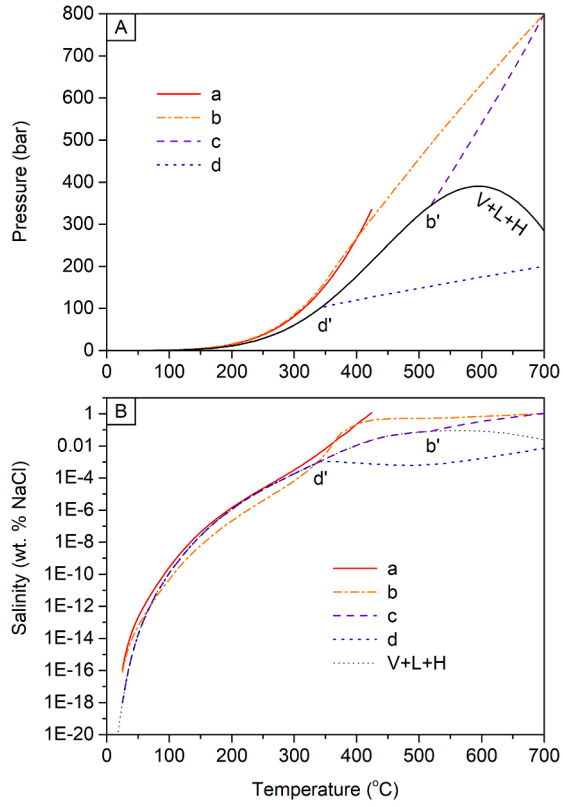

Fig. 4. Pressure–temperature and salinity-temperature paths for the vapor phases in fluid inclusions trapped at points a, b, c, and d in Fig. 1.

Sanchez et al., 2020; Zaheri-Abdehvand et al., 2020). The above complexity can be attributed to the phase relations in the H_2O-NaCl system and variable evolutionary paths after fluid entrapment at different conditions (Bodnar, 1994; Bodnar and Vityk, 1994; Wilkinson, 2001; Bodnar, 2003; Driesner and Heinrich, 2007; Lecumberri-Sanchez et al., 2012; Bodnar et al., 2014; Bakker, 2019; Becker et al., 2019; Klyukin et al., 2019).

The dominant components of aqueous fluids in the Earth's crust are H_2O, NaCl (or other salts), and CO_2 in varying proportions (Bodnar et al., 2014; Heinrich and Candela, 2014; Yardley and Bodnar, 2014). Therefore, the H_2O-NaCl system has been widely used in approximating fluid properties in natural systems, synthetic fluid inclusion studies, and numerical simulations (Bodnar, 1983; Bodnar, 1989; Heinrich et al., 1999; Ulrich et al., 2001; Weis et al., 2012; Bodnar et al., 2014; Weis et al., 2014; Tattitch and Blundy, 2017; Audétat, 2019). Various equations of state have been proposed to model fluid properties of the H_2O-NaCl system (Sourirajan and Kennedy, 1962; Hall et al., 1988; Bodnar, 1994; Bodnar and Vityk, 1994; Lecumberri-Sanchez et al., 2012). Models by Driesner and Heinrich (2007) and Driesner and Heinrich (2007) provide phase stability relations of the H_2O-NaCl system for temperatures from 0 to 1000 °C, pressures from 0 to 5000 bar, and compositions from 0 to 1 mol fraction of NaCl. Based on their equations, a series of previous studies conducted numerical calculations and provided deep insights into the properties of fluid inclusions in the H_2O-NaCl system (Lecumberri-Sanchez et al., 2012; Steele-MacInnis et al., 2012a; Steele-MacInnis et al., 2012b; Lecumberri-Sanchez et al., 2015a; Lecumberri-Sanchez et al., 2015b; Bakker, 2018; Bakker, 2019; Becker et al., 2019; Klyukin et al., 2019).

Fluids in the H_2O-NaCl system may experience complicated evolutionary paths to form fluid inclusions with distinctive phase ratios and microthermometric properties. Bodnar et al. (1985) demonstrated the bubble variation of an entrapped vapor phase from 700 ℃ and 700 bar to the ambient condition. Bodnar (1994) and Becker et al. (2008) illustrated the evolutionary paths for the formation of three types of halite-bearing fluid inclusions with characteristic homogenization behavior. Bodnar and Vityk (1994) illustrated the isochores for fluids with the salinity from 0 to 40 wt% NaCl. Bakker (2018) compiled the AqSo_NaCl program for the calculation of fluid properties and fluid inclusion evolutionary paths in the H_2O-NaCl system. Bakker (2019) considered the quartz volume modifications and presented corrected evolutionary paths for high salinity fluids that intersect the halite liquidus and Vapor + Liquid + Halite surface, respectively. Klyukin et al. (2019) reviewed the evolutionary paths and illustrated the phase characteristics from ambient temperature to homogenization for fluid inclusions trapped on or with isochores intersecting the Vapor + Liquid surface of the H_2O-NaCl system. Most previous fluid inclusion studies

Table 1
Calculated fluid inclusion properties corresponding to labeled points in Figs. 1 and 2.

Entrapment in the single-phase region	Point in Fig. 1		a	h	i	j	k	l	a_1 in Fig. 6A	i_1 in Fig. 8A	j_0 in Fig. 18
	Pressure	bar	2000	1124	2000	249.7	5000	2200	2000	2000	330
	Temperature	℃	700	900	900	900	792.4	1000	770.2	576.3	1000
	Salinity	wt. % NaCl	10	1.06	61.39	0.0073	84.97	30	10	50	0.1016
	Density	g/cm^3	0.599	0.229	1.04	0.0473	1.45	0.619	0.542	1.11	0.0573
Total homogenization	Point in Fig. 1		a'	b	c	d	f	m	a_1' in Fig. 6A	c' in Fig. 8A	d_0 in Fig. 18
	h-mode		VL-L*	VL-V	VLH-VL-L	VL-VH-V	VLH-LH-L	VLH-VL-V	VL-C	VLH-L	VL-VH-VL-V
	h-pressure	bar	334.4	800	800	200	2000	2065.7	462.7	212.5	300
	h-temperature	℃	424.1	700	700	700	700	967.3	464.5	424.6	900
Partial homogenization**	Point in Fig. 1				c'	d'	f'	m'			d_1, d_2 in Fig. 18
	ph-pressure	bar			344.1	102.1	360.3	4.4			243.6/123.2
	ph-temperature	℃			518.5	343.0	650.8	159.8			718.1/360.8
	Ice-melting	℃	−6.6	−0.6		−0.004			−6.6		−0.06
Room temperature phase ratios	Vol-halite	vol %	0	0	22.8	0	53.3	1.4	0	16.4	0
	Vol-solution	vol %	56	22.8	45.4	4.7	24.7	49.2	50.7	62.9	5.7
	Vol-bubble	vol %	44	77.2	31.8	95.3	22	49.4	49.3	20.7	94.3

Notes:
* V-vapor, L-liquid, H-halite, C-critical.
** Partial homogenization refers to the disappearance of vapor (f′), liquid (m′), or halite (c′) upon heating of these fluid inclusions. For fluid inclusions trapped at points j and j_0, partial homogenization refers to the appearance of halite at points d′ and d_2 and disappearance of halite at point d_1 upon heating.

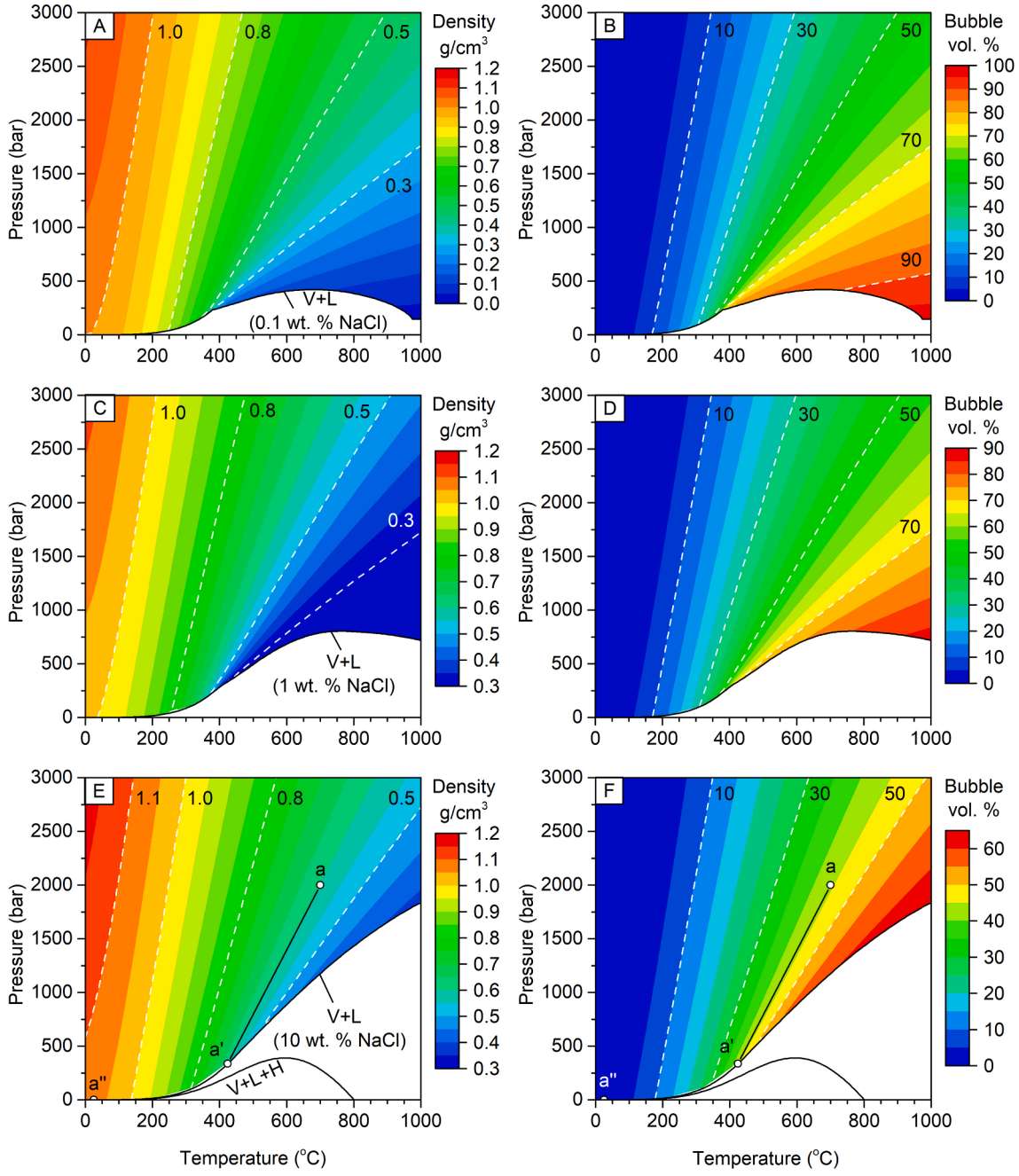

Fig. 5. Contour figures for the fluid density and room-temperature percentage of the vapor phase (bubble) of corresponding fluid inclusions at different salinities. Points a, a′ and a″ are consistent with those in Fig. 1.

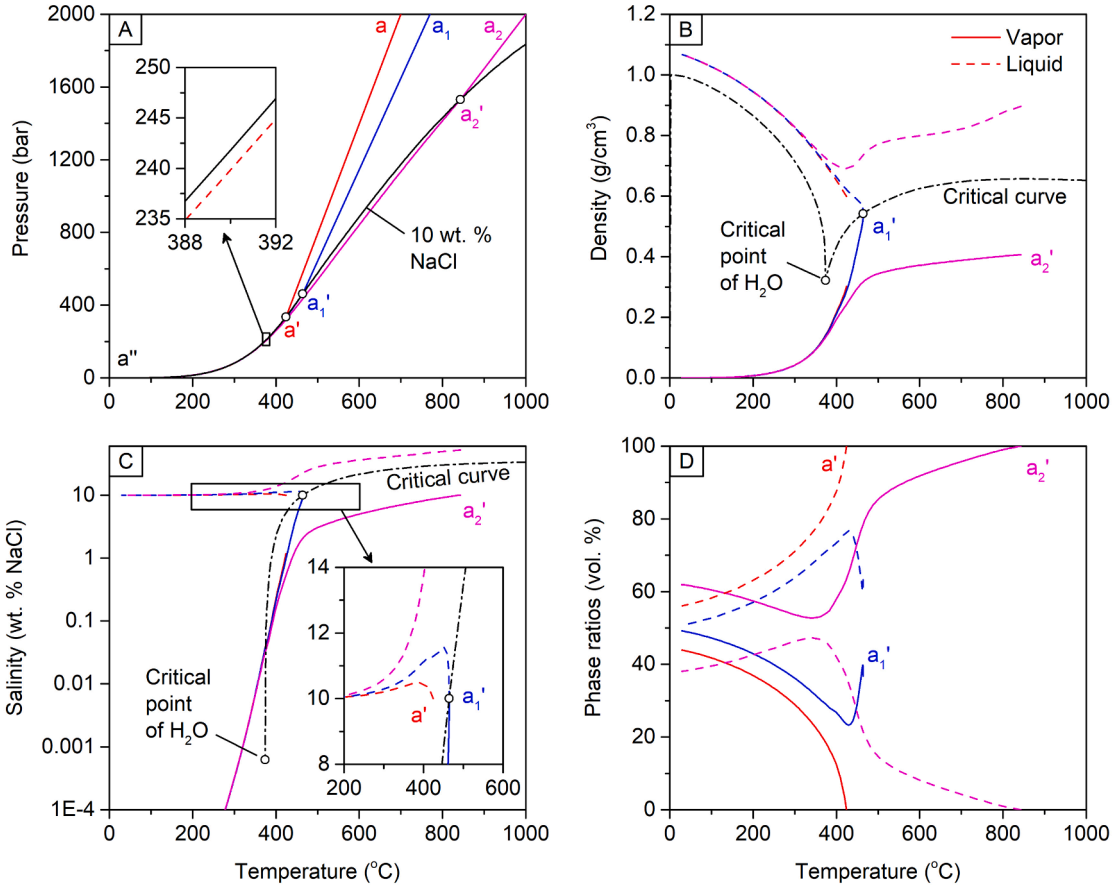

Fig. 6. Variations of fluid density, salinity, and fluid inclusion phase ratios with temperature for the 10 wt% NaCl solution. Dashed lines represent the liquid phases and solid lines represent the vapor phases. Entrapment conditions are 700 °C, 770.2 °C, and 1000 °C at pressure of 2000 bar for points a, a_1, and a_2, respectively. Evolution a-a′-a″ is consistent with that in Fig. 1 and intersect the V + L surface at the dew curve; evolution a_1-a_1′-a″ intersect the V + L surface at the critical curve; evolutions a_2-a_2′-a″ intersect the V + L surface at the bubble curve.

focused on fluid inclusions formed in the single-phase region, the two-phase (Vapor + Liquid) region, and on the halite liquidus of the H_2O-NaCl system. Little attention has been paid to the Vapor + Halite region, which corresponds to the very shallow magmatic-hydrothermal mineral deposits (Muntean and Einaudi, 2000; Kodera et al., 2014; Becker et al., 2019; Mernagh and Mavrogenes, 2019).

In this study, we present a systematic illustration of the fluid density, salinity, and room-temperature phase ratios of corresponding fluid inclusions with contour figures in the H_2O-NaCl system, a comprehensive construction of the evolutionary paths of fluids trapped at variable conditions, and a detailed discussion of the changes of fluid inclusion properties along these evolutionary paths. Our work reveals a new type of fluid inclusion that experiences partial homogenization by halite dissolution and total homogenization by liquid disappearance. A correction method is provided for the overestimated bulk salinity owing to the presence of vapor phase at the point of halite dissolution for halite-bearing fluid inclusions. We also demonstrate that vapor-rich fluid inclusions that formed in the Vapor + Halite region experience the transition of phases from vapor + liquid to vapor + halite before total homogenization. Our findings will expand these of earlier studies (Bodnar and Vityk, 1994; Becker et al., 2008; Steele-MacInnis and Bodnar, 2013; Bakker, 2018; Bakker, 2019; Becker et al., 2019; Klyukin et al., 2019) and facilitate the interpretation of fluid inclusion petrography, phase relations, and microthermometric results in the H_2O-NaCl system.

2. Methods

Figs. 1 and 2 show that three surfaces (vapor + liquid, vapor + liquid + halite, and halite liquidus surfaces) split the pressure–temperature-salinity phase diagram of the H_2O-NaCl system into 4 regions, namely single-phase, vapor + liquid, vapor + halite, and liquid + halite regions.

2.1. Phase ratios in fluid inclusions

A fluid inclusion in the H_2O-NaCl system may contain variable proportions of a vapor phase (V), a liquid phase (L), and a solid phase (H-halite) if the fluid is saturated with NaCl at a given pressure and temperature condition (Roedder, 1971). To quantify the volumes of the vapor, liquid, and halite at any point from entrapment to the ambient conditions, we conducted numerical calculations with the methods of Bodnar (1983), Bakker (2018, 2019), Becker et al. (2019), and Klyukin et al. (2019), assuming that the volume and mass of fluid inclusions are not modified after their entrapment (Bodnar, 2003).

(1) For a V + L type fluid inclusion at a given temperature,

$$v_{bulk} = v_{vapor} + v_{liquid} \quad (1)$$

$$m_{bulk} = \rho_{\text{vapor}} \times v_{vapor} + \rho_{liquid} \times v_{liquid} \quad (2)$$

$$m_{\text{bulk}}^{NaCl} = \rho_{\text{vapor}} \times v_{vapor} \times s_{vapor} + \rho_{liquid} \times v_{liquid} \times s_{liquid} \quad (3)$$

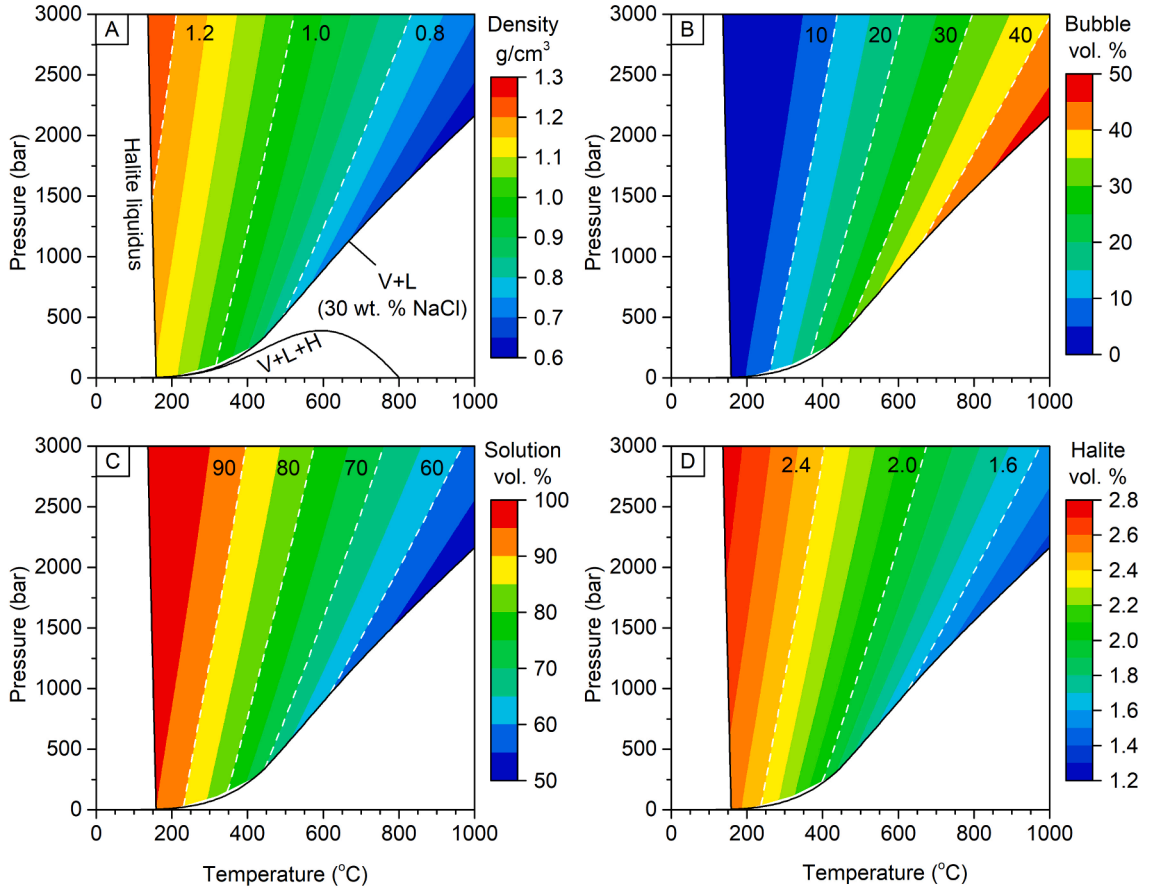

Fig. 7. Contour figures for the fluid density and room-temperature phase ratios of corresponding fluid inclusions at 30 wt% NaCl.

where v is volume, m is mass, ρ is density, and s is salinity.

Solving equations (1), (2), and (3) yields the volume of liquid and vapor phases as observed at a given temperature:

$$v_{\text{liquid}} = \frac{m_{bulk}^{NaCl} - m_{bulk} \times s_{vapor}}{\rho_{liquid} \times (s_{liquid} - s_{vapor})} \tag{4}$$

$$v_{\text{vapor}} = \frac{m_{bulk} - \rho_{liquid} \times v_{liquid}}{\rho_{vapor}} \tag{5}$$

Pressure is required to obtain the salinities and densities of the vapor and liquid phases in equations (2) to (5) at a given temperature. The maximum pressure is below the locus on the critical curve, while the minimum pressure is above the vapor + liquid + halite coexistence surface at given temperature (Figs. 2, 3). With a specified v_{bulk}, an iteration procedure is conducted to get the pressure so that the difference between the calculated $v_{vapor} + v_{liquid}$ and v_{bulk} is within tolerance (Klyukin et al., 2019). Then the density, salinity, and volume ratio of each phase can be obtained from equations in Driesner and Heinrich (2007) and Driesner and Heinrich (2007).

The calculations for a H + L type fluid inclusion (evolution along the halite liquidus: f-f′ in Fig. 1) or a V + H type fluid inclusion (evolution along the bubble curve of the V + H region: d-d′) are the same as for the V + L type, with the exception that either the subscript *"vapor"* or *"liquid"* is substituted by *"halite"* in equations (1) to (5).

(2) For a V + L + H type fluid inclusion at given temperature,

$$v_{bulk} = v_{vapor} + v_{liquid} + v_{halite} \tag{6}$$

$$m_{bulk} = \rho_{\text{vapor}} \times v_{vapor} + \rho_{liquid} \times v_{liquid} + \rho_{\text{halite}} \times v_{halite} \tag{7}$$

$$m\text{NaCl}_{bulk} = \rho_{\text{vapor}} \times v_{vapor} \times s_{vapor} + \rho_{liquid} \times v_{liquid} \times s_{liquid} + \rho_{\text{halite}} \times v_{halite} \times s_{halite} \tag{8}$$

The pressure is acquired on the vapor + liquid + halite coexistence surface at a given temperature (Figs. 1, 2, and 3), therefore, the volume ratio of each phase can be acquired by solving equations (6), (7), and (8).

2.2. Evolutionary paths of fluid inclusions

The fluids entrapped in the single-phase region will experience a two-stage evolutionary path (e.g., a-a′-a″ in Fig. 1) for halite-undersaturated H_2O-NaCl solutions (i.e., salinity ≤ 26.46 wt% NaCl at 25 °C), or a three-stage evolutionary path for halite-saturated solutions (e.g., i-c-c′-c″) and solutions with extremely low salinity (e.g., j-d-d′-d″). The first stage of the evolutionary paths for all solutions trapped in the single-phase region are the isochores (i.e., line of constant density). They intersect either the V + L surface (e.g., a-a′ in Fig. 1), the halite liquidus (e.g., k-f), or the bubble curve of the V + H region (e.g., j-d). At the point where the isochore intersects a phase boundary, the fluid has a salinity and density identical to the entrapped fluid in the single-phase region. A new phase (vapor, liquid, or halite) is produced at the intersection. Note that the nucleation of a new phase may occur at several degrees Celsius lower than the temperature at the intersect point (Sterner et al., 1988; Bodnar, 2003). We here ignore this delayed appearance of the new phase for simplicity. The second stage of the evolutionary paths for all

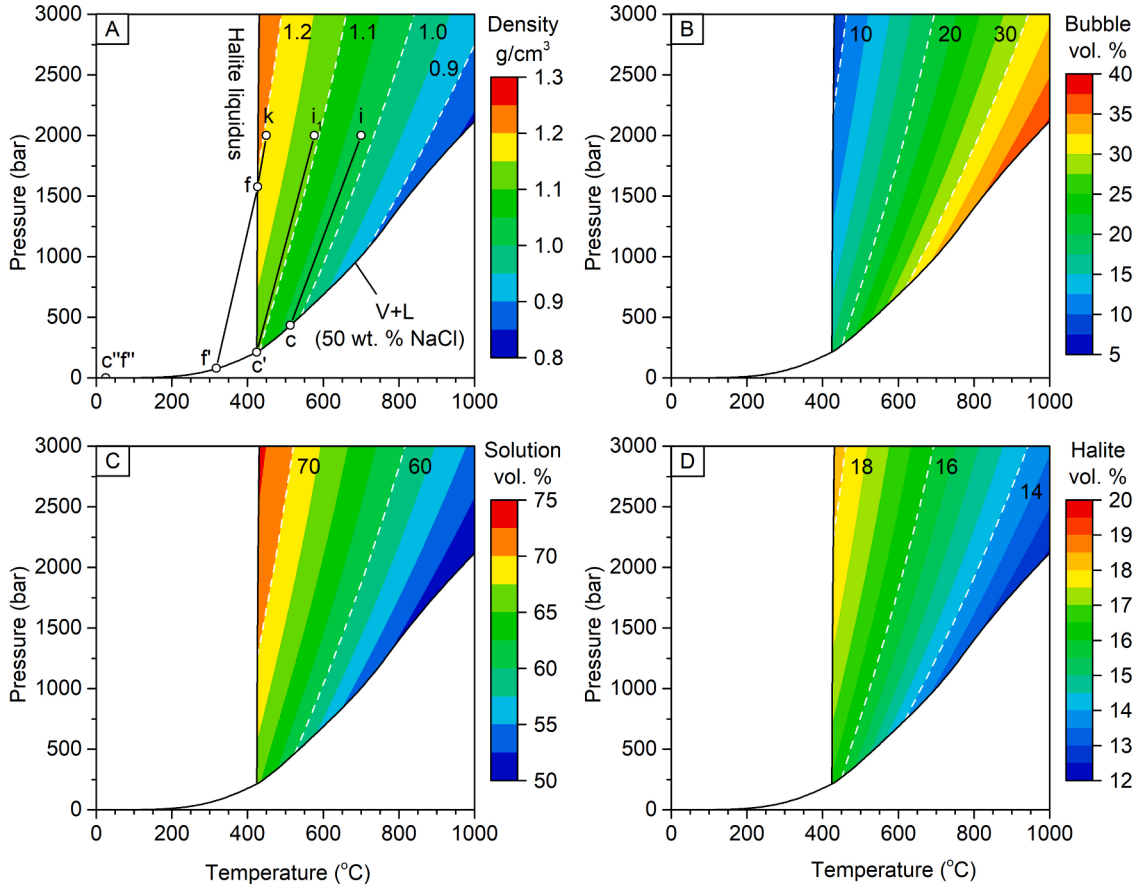

Fig. 8. Contour figures for the fluid density and room-temperature phase ratios of corresponding fluid inclusions at 50 wt% NaCl. Evolutions i-c-c′-c″ and k-f-f′-f″ represent the same evolution patterns as labeled in Fig. 1. Evolution for point i′ passes point c′ where halite and vapor emerge simultaneously.

solutions trapped in the single-phase region are in the two-phase regions (V + L, V + H, or L + H regions). The internal pressure of the fluid inclusions with two phases can be obtained from equations (1) to (5), therefore, the second stage of the evolutionary path and corresponding density, salinity, and volume ratios of the two phases can be calculated (Figs. 1, 4). The second-stage of the evolutionary paths for the halite-saturated solutions will intersect the dew curve of the V + L + H surface (e.g., point c′ in Fig. 1), and then follow it to room temperature. Therefore, the third stage of the evolutionary paths and density, salinity, and volume ratios of the three phases can be obtained from equations (6), (7), and (8). The second stage of the evolutionary paths for solutions with extremely low salinities will intersect the bubble curve of the V + L + H surface (e.g., point d′ in Fig. 1), and then enter the V + L region and evolve to room temperature. Therefore, the third stage of the evolutionary paths and corresponding density, salinity, and volume ratios of the two phases can be calculated with equations (1) to (5), (Figs. 1 and 4).

Note that the above calculations are based on the assumption of no volume and mass changes after entrapment of fluid inclusions. However, many studies found that post-entrapment modifications may significantly alter fluid inclusion shapes and compositions (Bakker and Jansen, 1990; Audétat and Günther, 1999; Tarantola et al., 2010; Lerchbaumer and Audétat, 2012; Tarantola et al., 2012; Audétat, 2023; Zhang and Audétat, 2023). Therefore, the readers are reminded not to simply use these ideal models, but to observe fluid inclusions to find suitable samples for analyses.

3. Results

Table 1 presents calculated properties of nine types of fluid inclusions with the H_2O-NaCl solution at variable conditions (points a, h, i, j, k, and l) in the single-phase region (Figs. 1 and 2). Evolutionary paths for three special types of fluid inclusions (points a_1, i_1, and j_0) are not labeled in Figs. 1 and 2 for simplicity. Where applicable, the salinity, density, phase ratios, homogenization and partial homogenization pressures and temperatures, homogenization mode, and ice-melting temperature are calculated for each fluid inclusion. Detailed data for the evolutionary paths are presented in Appendix A and plotted in Figs. 6, 12, 14, 16, and 18. Upon heating of these fluid inclusions, volume ratios of each phase change along these evolutionary paths, demonstrating distinctive homogenization behavior. For example, a V + L type fluid inclusion would homogenize to liquid at point a′ for fluid trapped at point a, to vapor at point a_2' for fluid trapped at point a_2, and by disappearance of the meniscus at point a_1' for fluid trapped at point a_1 (Fig. 6). A halite-bearing fluid inclusion may experience partial homogenization by halite dissolution at point c′ and total homogenization vapor disappearance at point c (Figs. 1, 12), or partial homogenization by halite dissolution at point m′ and total homogenization by liquid disappearance at point m (Figs. 1, 14), or partial homogenization by vapor disappearance at point f′ and total homogenization by halite dissolution at point f (Figs. 1, 16). Upon heating, vapor ratio of the fluid inclusion trapped at point l firstly decreases from nearly ~ 49 vol% to 38 vol% at 420 °C, then increases to ~ 68 vol% at 950 °C, and then it sharply increases to 100 vol% at 968 °C (Figs. 1, 14D; Appendix A;

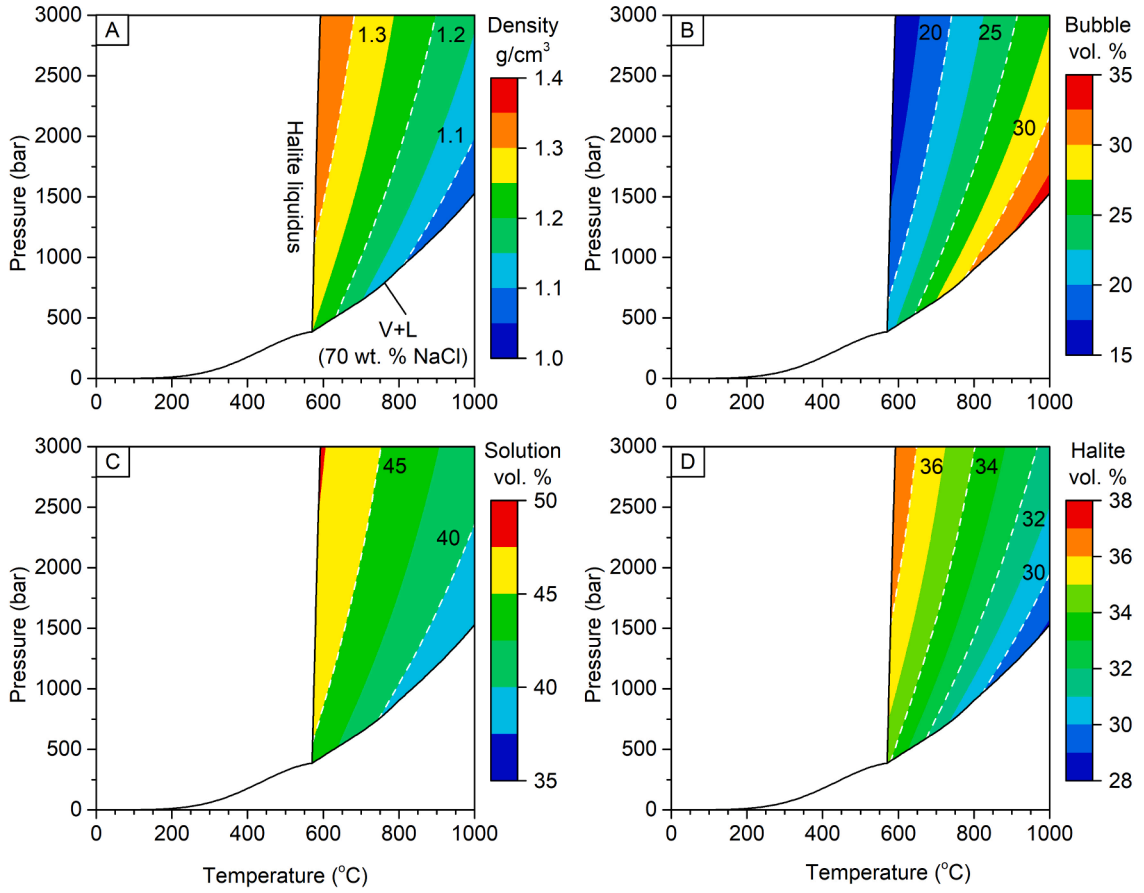

Fig. 9. Contour figures for the fluid density and room-temperature phase ratios of corresponding fluid inclusions at 70 wt% NaCl.

Homogenization by inversion: the bubble volume firstly decreases and then increases upon heating, Ermakov, 1965).

Contour figures are constructed in the pressure–temperature projection for fluid salinities at 0.1, 1, 10, 30, 50, and 70 wt% NaCl, for the bubble curve and the dew curve, and for the halite liquidus of the H_2O-NaCl system to demonstrate the variations of fluid salinities, densities and room-temperature phase ratios (Figs. 5, 7–11, 15, and 17). Multiple evolutionary paths are constructed in some contour figures to show the variations leading to different microthermometry behavior in fluid inclusions.

Owing to the presence of residual low-salinity vapor phase, salinity obtained at partial homogenization temperature by halite dissolution is consistently higher than the bulk fluid salinity (Steele-MacInnis and Bodnar, 2013). Therefore, we tabulated the data of the overestimation of bulk salinity in Table 2. It can be used for a convenient correction when necessary. Within our calculation range, the largest overestimation reaches 1.9 wt% NaCl at 1000 °C for the 55 wt% NaCl solution (Fig. 13).

4. Discussion

4.1. Single-phase region (Halite-undersaturated)

Contour figures constructed at three salinities (0.1 wt%, 1 wt%, and 10 wt% NaCl) demonstrate that slopes of the isochores in the pressure–temperature diagrams are essentially linear in the single-phase region (Bodnar and Vityk, 1994), except for the very low temperature regions (Fig. 5; Bakker, 2019). This feature is inherited from the generally linear isochores of pure H_2O and NaCl, because the density of the H_2O-NaCl system is calculated by the linear conversion of the pure water system (equations (7) and (8) in Driesner and Heinrich, 2007). The isochores generally move toward the higher temperature region with the increase of bulk fluid salinity, because NaCl has consistently higher density than H_2O. At a given pressure, the size of the vapor phase (bubble) in a fluid inclusion at ambient temperature increases with increasing temperature. The largest bubble size occurs at the high-temperature and low-pressure region corresponding to the lowest density and is approximately 100 vol% for the 0.1 wt% NaCl solution, ~88 vol% for the 1 wt% NaCl solution, and ~65 vol% for the 10 wt% NaCl solution (Fig. 5B, D, F).

Entrapped fluids along each isochore in the single-phase region will produce fluid inclusions with the same bubble ratio at room temperature. Entrapment of the halite-undersaturated single-phase fluid will follow the isochores and intersect the V + L surface on the dew curve, the bubble curve, or the locus of the critical curve, depending on the pressure, temperature, and salinity of entrapped fluid (Fig. 6). For example, evolutionary path a-a′-a″ starts at 700 °C, 2000 bar, and 10 wt % NaCl and intersects the V + L surface on the dew curve at ~424 °C and ~334 bar (point a′), thereafter, it follows the V + L surface to room temperature at ~0.028 bar (Fig. 3). The internal fluid pressure is slightly lower than the pressure of the V + L surface at 10 wt% NaCl from point a′ to a″ (inset in Fig. 6A). Upon touching the V + L surface, a low-density and low-salinity vapor phase is separated to form a tiny vapor bubble in the fluid inclusion. Because H_2O preferentially partitions to the vapor phase compared to NaCl (Klyukin et al., 2019), the salinity of the liquid phase increases from 10 wt% NaCl to a maximum of ~10.5 wt% NaCl at ~389 °C, and then it decreases to approach 10 wt% at room temperature

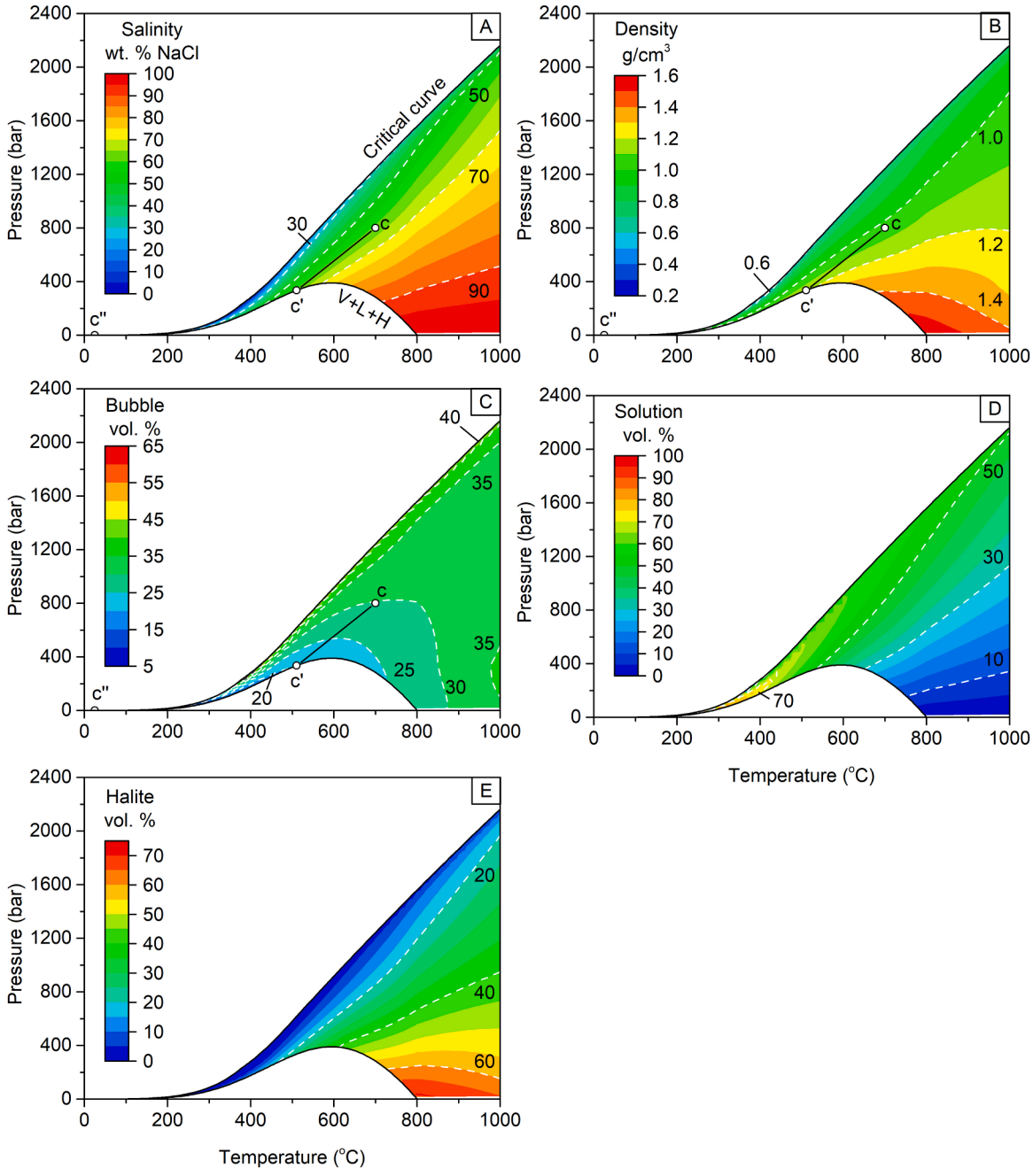

Fig. 10. Contour figures for the fluid salinity, density, and room-temperature phase ratios of corresponding fluid inclusions on the dew curve of the V + L surface. Evolution c-c′-c″ is consistent with that in Fig. 1.

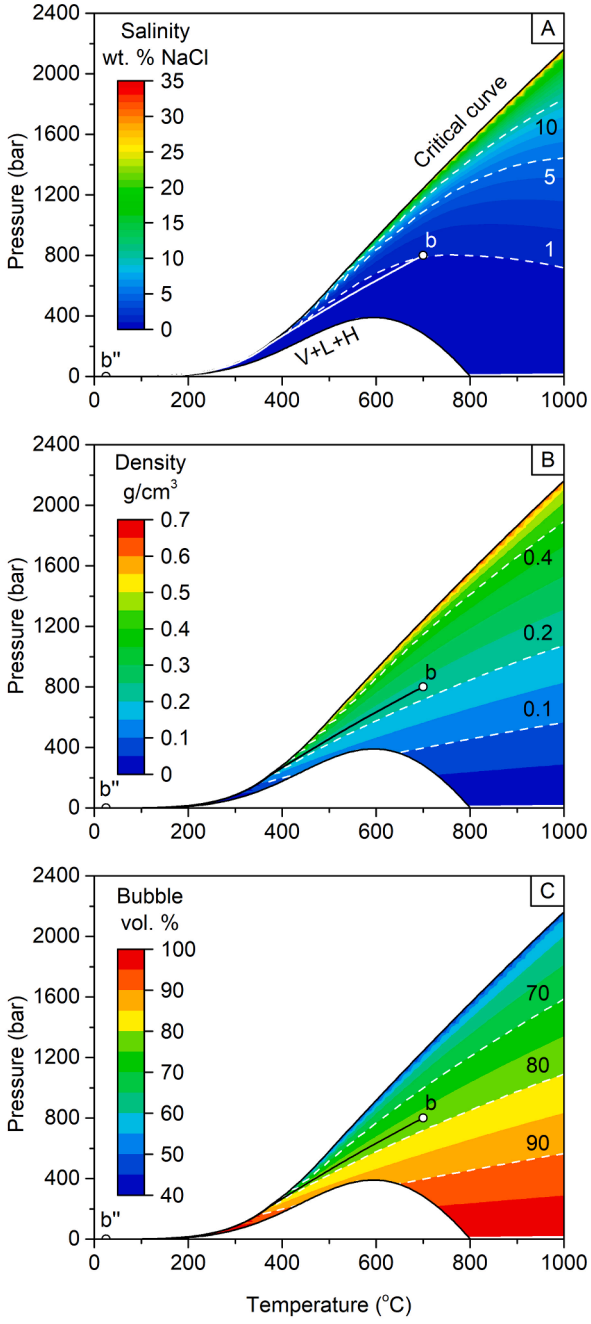

Fig. 11. Contour figures for the fluid salinity, density, and room-temperature phase ratios of corresponding fluid inclusions on the bubble curve of the V + L surface. Evolution b-b″ is consistent with that in Fig. 1.

(Fig. 6). Meanwhile, the salinity of the vapor phase decreases from ~1.2 wt% NaCl at point a′ to 1.13×10^{-16} wt% NaCl at room temperature (Fig. 4). The evolutionary path a-a′-a″ will form a V + L type fluid inclusion with a bubble content of 44 vol%. Upon heating, it will homogenize at point a′ by disappearance of the vapor phase.

The evolutionary path a_1-a_1′-a″ in Fig. 6 starts at 770 ℃, 2000 bar, and 10 wt% NaCl and intersects the V + L surface at the critical point at ~465 ℃ and ~463 bar (point a_1′; Table 1). After point a_1′, density and salinity of the vapor and liquid phases diverge to evolve to room temperature. The salinity of the liquid phase increases from 10 wt% NaCl to a maximum of ~11.6 wt% NaCl at ~451 ℃, then it decreases to approach 10 wt% at room temperature (inset in Fig. 6C). The evolutionary path a_1-a_1′-a″ will form a V + L type fluid inclusion with a bubble content of 49 vol%. Upon heating, the vapor phase firstly decreases to a minimum of ~23 vol% at ~430 ℃ and then increases to ~37 vol% at point a_1′ (Fig. 6D). The densities of the vapor and liquid phases become the same at point a_1′, so that this type of fluid inclusions homogenizes by disappearance of the meniscus (Knight and Bodnar, 1989; Klyukin et al., 2019).

The evolutionary path a_2-a_2′-a″ in Fig. 6 starts at 1000 ℃, 2000 bar, and 10 wt% NaCl and intersects the V + L surface on the bubble curve at ~843 ℃ and ~1530 bar (point a_2′). Upon touching the V + L surface, a high-density and high-salinity liquid phase is condensed in the fluid inclusion. After point a_2′, the evolution of the density and salinity of the vapor and liquid phases are generally parallel to the critical curve of the H_2O-NaCl system until the liquid density reaches a minimum of 0.69 g/cm^3 at ~420 ℃. Thereafter, the vapor and liquid phases diverge to evolve to room temperature (Fig. 6B). The salinity of the vapor phase decreases from 10 wt% NaCl to 1.13×10^{-16} wt% NaCl at room temperature (Fig. 4), while the salinity of the liquid phase decreases from 52.1 wt% NaCl to approach 10 wt% NaCl at room temperature (Fig. 6C). The evolutionary path a_2-a_2′-a″ will form a V + L type fluid inclusion with a bubble amount of ~62 vol%. Upon heating, the vapor phase firstly decreases to a minimum of ~52 vol% at ~334 ℃ and then increases to occupy the whole fluid inclusion at point a_2′ (Fig. 6D). Continuous heating of the above fluid inclusions will follow the isochores into the single-phase region (Figs. 1, 6A).

4.2. *Single-phase region (Halite-saturated)*

Halite saturation in fluid inclusions occurs above 26.46 wt% NaCl at room temperature. Figs. 7, 8, and 9 demonstrate that the isochores for high-salinity fluids have slight curvature to the high-temperature and low-pressure region (lower-right corner of each diagram). For a halite-saturated solution at a given pressure, the lower entrapment temperature will produce a fluid inclusion with a larger volume ratio of halite (e.g., Fig. 8D). The highest halite to vapor ratio occurs in the low-temperature and high-pressure region. Entrapment of the halite-saturated single-phase fluid will produce three types of V + L + H fluid inclusions with distinctive homogenization behavior, depending on the pressure, temperature, and salinity of entrapped fluid (Fig. 8A; Becker et al., 2008; Bodnar, 1994). Upon heating, fluid inclusions trapped at point i will show halite dissolution at point c′ and bubble disappearance at point c; fluid inclusions trapped at point k will show bubble disappearance at point f′ and halite dissolution at point f; fluid inclusions trapped at point i_1 will show simultaneous halite dissolution and bubble disappearance at point c′ (Table 1). Detailed evolutionary paths of the three phases in the V + L + H type inclusions are discussed in section 4.3 and 4.4.

Halite-bearing fluid inclusions with final homogenization by halite dissolution have been extensively reported in magmatic-hydrothermal deposits (Bodnar, 1994; Audétat and Günther, 1999; Becker et al., 2008; Rusk et al., 2008; Lecumberri-Sanchez et al., 2015a; Lecumberri-Sanchez et al., 2015b; Li et al., 2017; Zaheri-Abdehvand et al., 2020). Such fluid inclusions can be generated by (1) homogeneous entrapment of high-salinity fluid at very high-pressure conditions (Roedder and Bodnar, 1980; Bodnar, 1994), (2) accidental entrapment of excess halite with the saturated fluid (Becker et al., 2008; Lecumberri-Sanchez et al., 2012, 2015), or (3) post-entrapment modification such as H_2O loss and/or volume reduction (Audétat and Günther, 1999; Audétat, 2023; Audétat and Zhang, 2023). Points i and i_1 in Fig. 8 have the densities of 1.023 g/cm^3 and 1.109 g/cm^3, respectively, therefore, >8 % decrease of the fluid inclusion volume after entrapment at point i is sufficient to change the homogenization behavior. The compression of fluid trapped at point i to point k leads to the density increase to 1.195 g/cm^3, bubble decrease from 24 vol% to 12 vol%, and halite increase from 15.1 vol% to 17.7 vol%. Thus, these contour figures can facilitate the understanding of post-entrapment shrinkage or expansion of fluid inclusions which

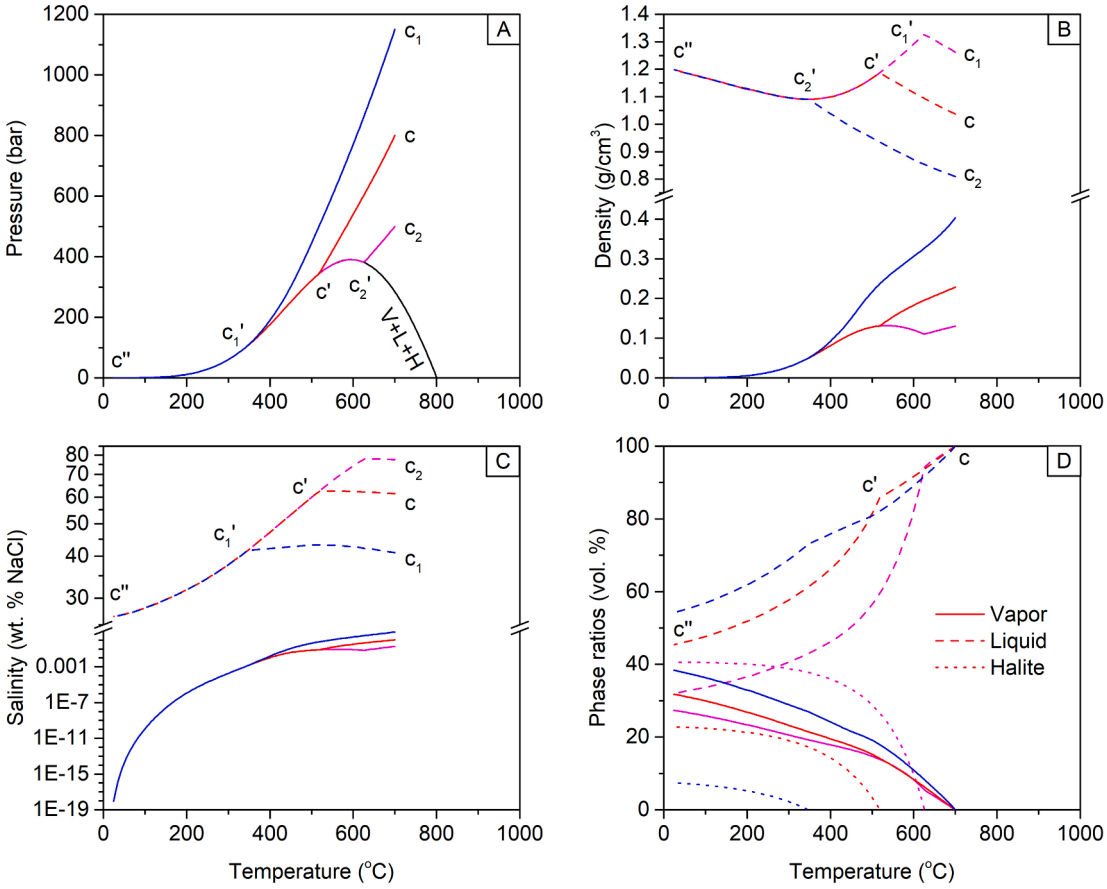

Fig. 12. Variations of fluid density, salinity, and fluid inclusion phase ratios with temperature for point c on the dew curve of the V + L surface.

alters fluid inclusion phase ratios and homogenization behavior.

4.3. *Vapor + liquid region*

Fig. 10 demonstrates that isolines for salinity and density on the dew curve of the V + L surface have notable curvatures. The consistent pattern for the contours of density and halite ratio demonstrates that NaCl dominates the variation of bulk fluid density (Fig. 10B, E). Consequently, the highest density occurs in the high-temperature and low-pressure region of the dew curve of the V + L surface. Fig. 11 demonstrates that the bubble curve has distinctive isoline patterns for the bulk fluid salinity, density, and bubble ratio compared to the dew curve. In the relatively high salinity region (e.g., 10 wt% NaCl) of the bubble curve, isochores and *iso*-salinity lines have consistent curvature, but the isochores are essentially linear in the relatively low-salinity region, because NaCl has less impact on the density of the low-salinity solution.

A 10 wt% NaCl solution at 800 bars and 700 ℃ lies in the liquid + vapor region, so it will split into 14.8 % mass proportions of brine with a salinity of ~61.4 wt% NaCl and 85.2 % mass proportions of vapor with a salinity of ~1.1 wt% NaCl (points c and b in Figs. 1 and 2). Evolution of the entrapped high-salinity fluid at point c will intersect the dew curve of the V + L + H surface at point c′ (344 bar and 519 ℃), and then follow the V + L + H surface to room temperature at ~0.019 bar (Figs. 3 and 10). After cooling from point c, a low-density and low-salinity vapor phase (point b) is separated to form a tiny vapor bubble in the fluid inclusion (Fig. 12). Owing to the stronger partitioning of H_2O into the vapor phase compared to NaCl, the salinity of the liquid phase increases from ~61.4 wt% NaCl to ~62.5 wt% NaCl at point c′. Thereafter, halite saturation is achieved to remove NaCl from the liquid phase so that its salinity decreases to 26.46 wt% NaCl at room temperature (Fig. 12C). Meanwhile, the salinity of the vapor phase decreases from ~1.1 wt% NaCl at point b to 0.08 wt% NaCl at point b′ on the bubble curve of the V + L + H surface and to 9.4 × 10^{-19} wt% NaCl at room temperature (Figs. 1, 4). The evolutionary path c-c′-c″ will form a V + L + H type fluid inclusion with the bubble filling 32 vol%, the liquid of 45 vol%, and halite of 23 vol%. Upon heating, halite disappears at point c′ and then the vapor phase disappears at point c. Continuous heating will follow the isochore c-i into the single-phase region (Fig. 1).

Salinity obtained at point c′ is typically taken as the bulk fluid salinity for halite-bearing fluid inclusions. However, Fig. 12C clearly demonstrates that bulk salinity at point c is notably lower than point c′. Steele-MacInnis and Bodnar (2013) demonstrated that mass in the vapor bubble cannot be neglected because it might have notable influence on the bulk fluid salinity when there is a large difference between the halite dissolution temperature and the vapor disappearance temperature. Density, salinity, and volume ratio of the vapor phase at point c′ are ~0.13 g/cm^3, ~0.08 wt% NaCl, and ~14 vol%, respectively (Fig. 12). Therefore, the salinity of the liquid phase is elevated from ~61.4 wt% NaCl at point c to ~62.5 wt% NaCl at point c′, and even higher salinity may occur along the V + L surface (e.g., c_1-c_1′ in Fig. 12C). The corresponding halite dissolution temperature is elevated to 519 ℃ compared to temperature on the dew curve of the V + L + H surface at bulk fluid salinity (511 ℃, Fig. 13A). The highest overestimation of bulk fluid salinity is >3 % and occurs in the high temperature region within the salinity range between 50 and 60 wt% NaCl (Fig. 13B, C), so that a

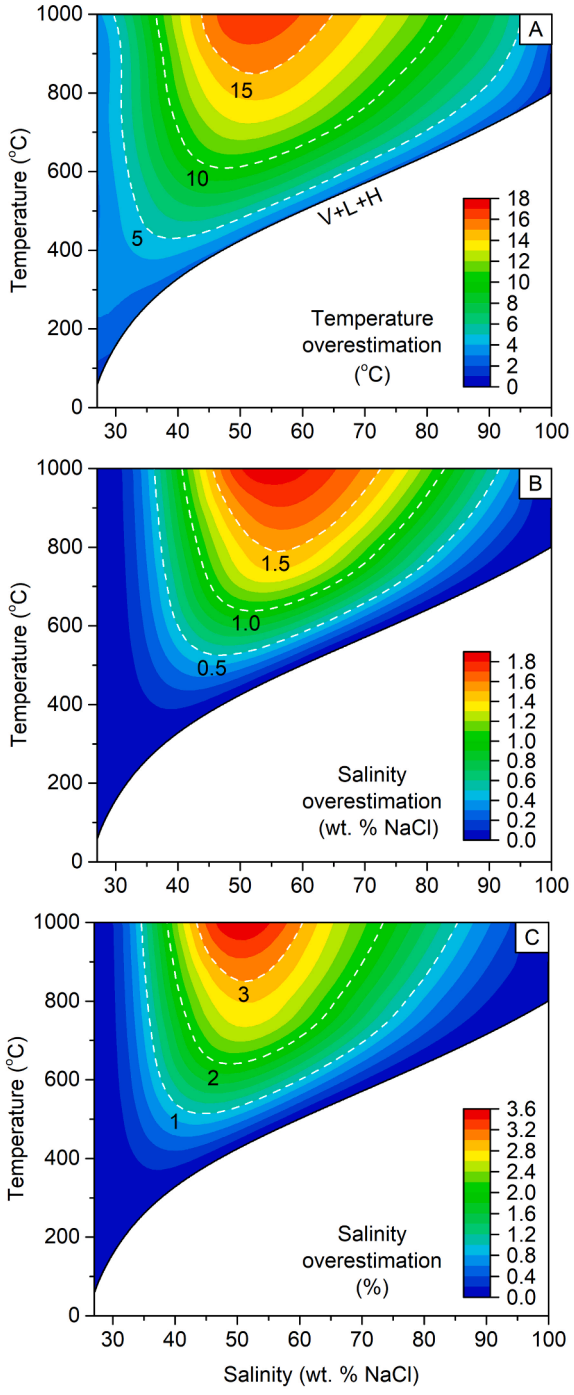

Fig. 13. Temperature and salinity overestimation at partial homogenization by halite dissolution. (A) The difference between halite dissolution temperature and temperature of the V + L + H surface at bulk fluid salinity. (B) The difference between apparent salinity obtained from halite dissolution temperature and bulk fluid salinity. (C) Percentage of salinity overestimation.

correction is required to eliminate salinity overestimation. With the apparent salinity obtained from halite dissolution temperature and the total homogenization temperature, correction can be conveniently conducted with Table 2. For example, if an apparent salinity obtained from halite dissolution temperature is 51.6 wt% NaCl and the total homogenization temperature is 900 °C, then the bulk fluid salinity should be corrected to 50.0 wt% NaCl.

Evolution of the entrapped low-salinity fluid at point b will not intersect the V + L + H surface (Fig. 14A; Klyukin et al., 2019), but will follow the V + L surface from point b to b″ at room temperature at ~0.031 bar (Fig. 3). After cooling from point b, a high-density and high-salinity liquid phase is condensed in the fluid inclusion. Evolution of the salinity and density of the vapor and liquid phases are generally parallel to the critical curve of the H_2O-NaCl system until the liquid density reaches a minimum of 0.58 g/cm^3 at ~370 ℃ (Fig. 14B). Thereafter, the vapor and liquid phases diverge to evolve to room temperature. The salinity of the vapor phase decreases from 1.1 wt% NaCl to 7.9 × 10^{-17} wt% NaCl at room temperature (Fig. 4), while the salinity of the liquid phase decreases from 61.4 wt% NaCl to approach 1.1 wt% NaCl at room temperature (Fig. 14C). Evolutionary path b-b″ will form a V + L type fluid inclusion with a bubble content of 77 vol%. Upon heating, the vapor phase firstly decreases to a minimum of ~73 vol% at ~290 ℃ (homogenization by inversion) and then increases sharply to > 95 vol% at 390 ℃. Thereafter, the proportion of vapor increases to a plateau stage and underestimation of homogenization temperature when doing microthermometry analysis is very likely to occur because of the difficulty to identify the disappearance of the last drop of liquid (Fig. 14D; Bodnar et al., 1985). Continuous heating will follow the isochore b-h into the single-phase region (Fig. 1).

The entrapped vapor phase typically evolves to a V + L type fluid inclusion that homogenizes by the disappearance of liquid, except for the halite-saturated region on the bubble curve of the V + L surface at high temperature and pressure conditions. The majority of the entrapped H_2O and NaCl will be converted into the liquid phase at room temperature, so that the salinity of the liquid phase will approach the bulk salinity (Fig. 6C, Fig. 14C). After a plateau stage, the sudden drop of the salinities of the vapor and liquid phases occurs around the critical point of pure water. The density of the liquid phase reaches a minimum around the critical point of pure water, corresponding to the rapid change of the volume ratio of the vapor phase (Fig. 14B, D).

The critical point of the H_2O-NaCl system has a salinity of ~26.5 wt% at 696 ℃, therefore, the entrapped fluid with an isochore intersecting the bubble curve at > 696 ℃ will evolve to be a V + L + H type fluid inclusion (Fig. 1). For example, evolutionary path l-m-m′-m″ starts at 1000 ℃, 2200 bar, and 30 wt% NaCl and intersects the V + L surface on the bubble curve at ~967℃ and ~2066 bar (point m), thereafter, it follows the V + L surface and intersects the V + L + H surface at ~160 ℃ and ~4.4 bar (point m′), and then evolves to room temperature at ~0.019 bar (Fig. 3). Upon touching the V + L surface, a slightly higher-density and higher-salinity liquid phase is condensed in the fluid inclusion (Fig. 14). Owing to the preferential partition of NaCl to the liquid phase compared to H_2O, the salinity of the liquid phase increases from 33.6 wt% at point m to 42.4 wt% NaCl at ~833 ℃, and then it decreases to approach 30 wt% NaCl until point m′ on the V + L + H surface. Then salinity of the liquid phase decreases to 26.46 wt% NaCl at room temperature. Meanwhile, the salinity of the vapor phase decreases from 30 wt% NaCl at point m to 9.4 × 10^{-19} wt% NaCl at room temperature (Fig. 14). The evolutionary path l-m-m′-m″ will form a V + L + H type fluid inclusion with the bubble filling 49.4 vol%, the liquid of 49.2 vol%, and halite of 1.4 vol%. Homogenization by inversion will also be observed upon heating of such a fluid inclusion. Its halite disappears at point m′ and then the liquid phase disappears at point m. Continuous heating will follow the isochore m-l into the single-phase region (Fig. 1).

4.4. *Liquid + halite region*

The *iso*-salinity lines on the halite liquidus are generally vertical, with slightly negative slopes in the low-temperature region and positive slopes in the high-temperature region (Fig. 15A; Bodnar, 1994; Becker et al., 2008), consistent with the isolines for the room-temperature halite ratio (Fig. 15E). In contrast, the isochores on the halite liquidus display an anticlinal shape, with the lowest value in the temperature range of 300 to 400 ℃ at pressure below 250 bar (Fig. 15B). The increased salinity dominates the density on the halite liquidus at high temperature

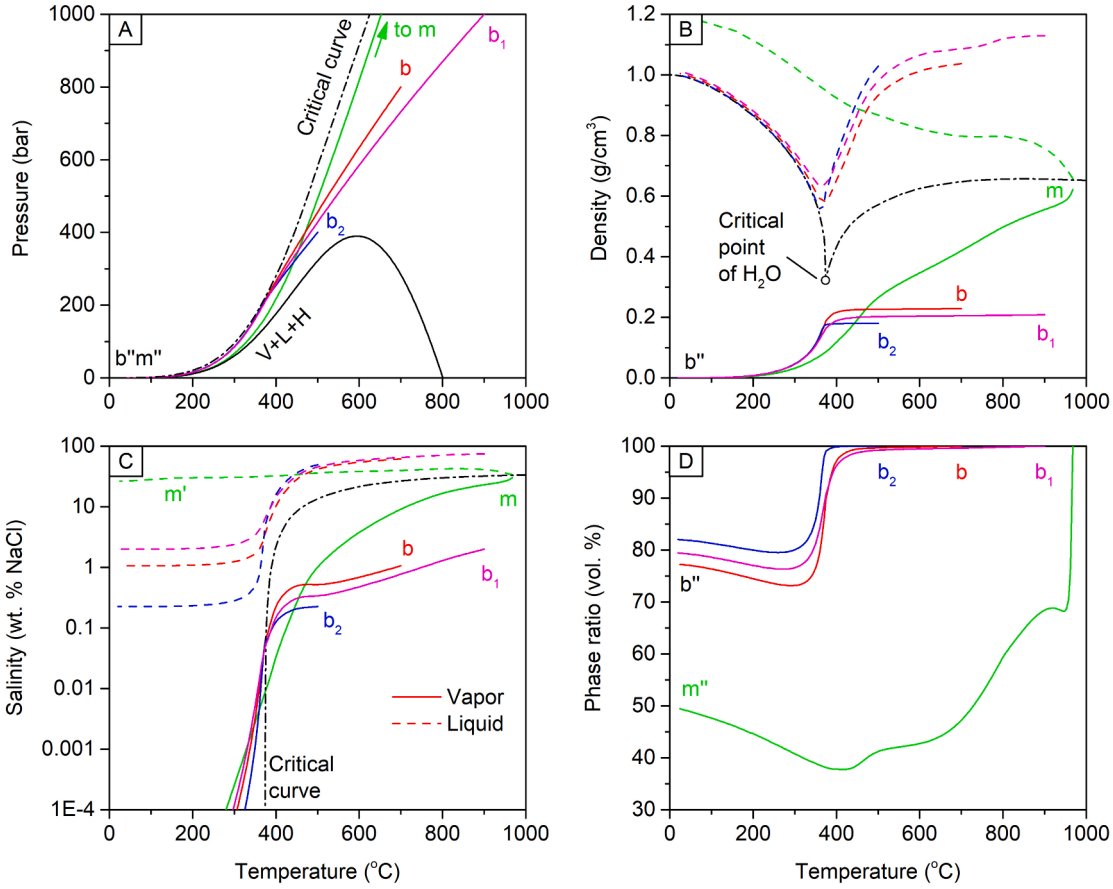

Fig. 14. Variations of fluid density, salinity, and fluid inclusion phase ratios with temperature for points b and m on the bubble curve on the V + L surface.

and reverses the slopes of the isochores. The pressure–temperature projections of the evolutionary paths along the halite liquidus show notable curvature (Fig. 16A), because of the change of fluid density and salinity.

A 90 wt% NaCl solution at 2000 bars and 700 ℃ lies in the liquid + halite region, so it will split into 66.5 % mass proportions of brine with salinity of ~85.0 wt% NaCl and 33.5 % mass proportions of halite (points f and g in Figs. 1, 2). Evolution of the entrapped high-salinity fluid at point f will intersect the dew curve of the V + L + H surface at point f′ (360 bar and 651 ℃), and then follow the V + L + H surface to room temperature at ~0.019 bar (Figs. 4, 15). After cooling from point f, halite is continuously saturated from the solution so that its salinity decreases to 26.46 wt% NaCl at room temperature (Fig. 16A). The density of the liquid phase decreases from 1.55 g/cm^3 at point f to a minimum of 1.09 g/cm^3 at ~348 ℃ and then increases to 1.20 g/cm^3 at room temperature (Fig. 16B). A vapor phase appears after the fluid cools to point f′. The salinity of the vapor phase increases from 0.068 wt% NaCl to a maximum of ~0.92 wt% NaCl at 563 ℃ and the vapor density increases from 5.0 × 10^{-4} g/cm^3 to a maximum of ~0.13 g/cm^3 at 535 ℃, and then it decreases to 9.4 × 10^{-19} wt% NaCl and 1.4 × 10^{-5} g/cm^3 at room temperature, respectively. The evolutionary path f-f′-f″ will form a V + L + H type fluid inclusion with a bubble content of 22 vol%, liquid content of 25 vol%, and halite content of 53 vol% (Fig. 16D). Upon heating, the vapor phase disappears at point f′ and then the halite disappears at point f. Continuous heating will follow the isochore f-k into the single-phase region (Fig. 1).

4.5. *Vapor + halite region*

The addition of trace amount of NaCl will significantly alter the phase relationship of H_2O (Bodnar and Vityk, 1994; Driesner and Heinrich, 2007; Bakker, 2019). Fig. 17 shows that *iso*-salinity lines of the vapor phase in the V + H region generally display a concentric pattern with the lowest values in the low-temperature and low-pressure region. At a given temperature, the salinity of the vapor phase increases dramatically to approach 100 wt% NaCl at very low pressure close to the halite sublimation curve (Driesner and Heinrich, 2007). Therefore, data below 1 bar are not included for a better demonstration of the contour figures. In contrast to the curved *iso*-salinity lines, isochores and *iso*-bubble lines for the vapor phase are generally linear, because trace amount of NaCl has a trivial influence on the density of the vapor phase. There is a smooth transition from the bubble curve of the V + L region to the V + H region (Fig. 17).

A 10 wt% NaCl solution at 200 bar and 700 ℃ lies in the vapor + halite region, so it will split into 90.0 % mass proportions of vapor with a salinity of ~0.0073 wt% NaCl and 10.0 % mass proportions of halite (points d and e in Figs. 1, 2). Evolution of the entrapped vapor phase at point d will intersect the bubble curve of the V + L + H surface at point d′ (343 ℃, 102 bar), and then enters the V + L region and evolve to room temperature at 0.031 bar (Fig. 17). After cooling from point d, halite is continuously saturated from the vapor. The volume ratio of halite increases to a maximum of 1.55 × 10^{-4} vol% at ~495 ℃ and then decreases to 1.39 × 10^{-4} vol% at point d′. The salinity of the vapor phase decreases to a minimum of 6.20 × 10^{-4} wt% NaCl at ~485 ℃ and then increases to 1.16 × 10^{-3} wt% NaCl at point d′ (Fig. 4). The vapor density

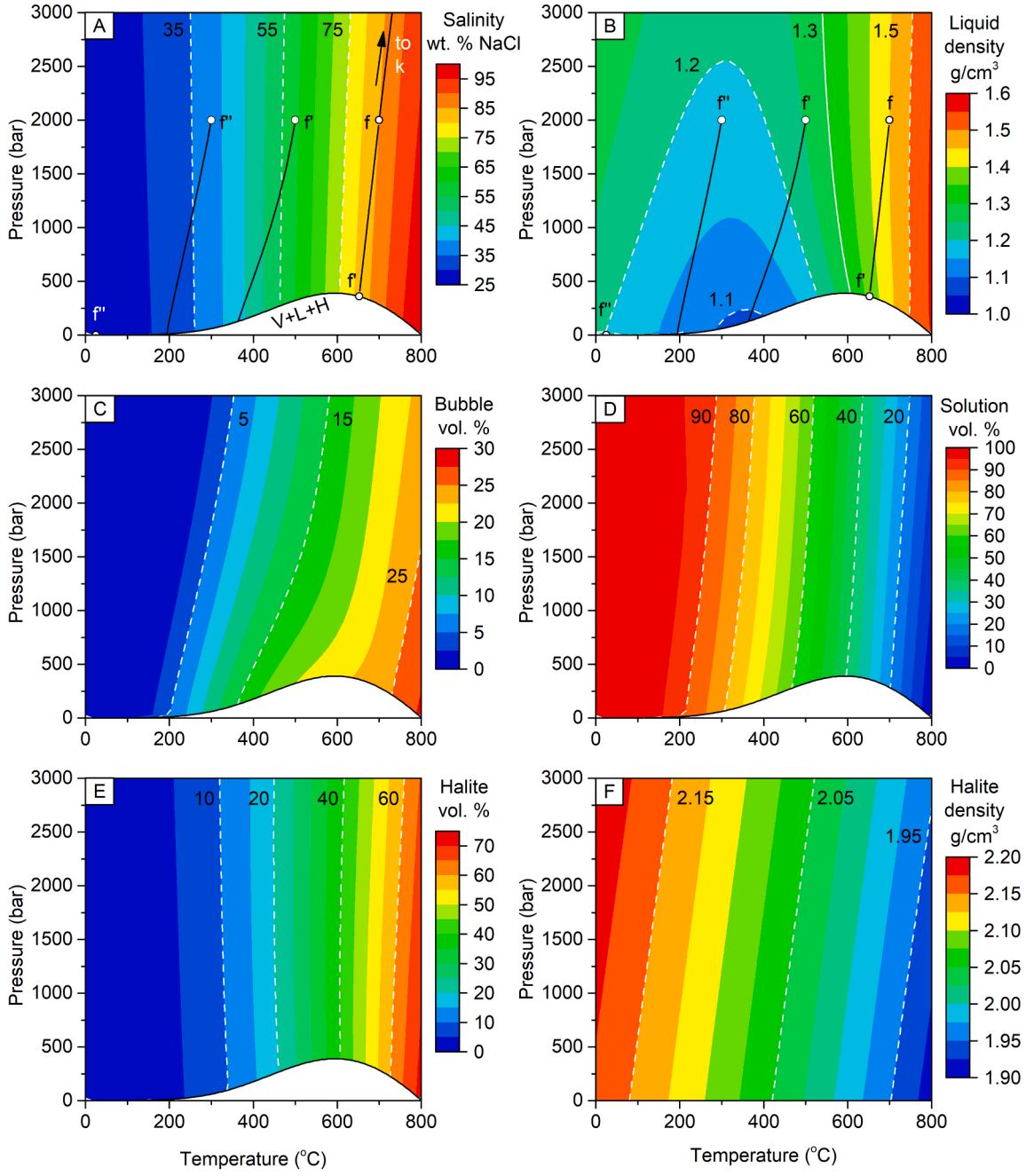

Fig. 15. Contour figures for the fluid salinity, density, and room-temperature phase ratios of corresponding fluid inclusions on the halite liquidus. Evolution f-f′-f″ is consistent with that in Fig. 1.

remains almost constant at ~0.047 g/cm^3 from d to d′ (Fig. 18B), because the vapor salinity is so low that its density is determined by the H_2O content rather than the NaCl content.

There is the coexistence of vapor, halite-saturated liquid, and halite at point d′. After cooling from point d′, the halite is consumed and the following evolution is consistent to inclusions trapped on the bubble curve of the V + L surface (Figs. 14, 18; Bakker, 2018, 2019). Thereafter, the majority of the H_2O and NaCl is converted into the halite-undersaturated liquid phase with high density and salinity, so the density and salinity of the vapor phase decrease dramatically during cooling to room temperature (Fig. 18). The volume of the vapor phase decreases to a minimum of ~95.1 vol% at ~130 °C and then increases to 95.3 vol% at room temperature. Evolution d-d′-d″ will form a V-L type fluid inclusion with the bubble ratio of 95.3 vol% (Fig. 18D). Upon heating, the vapor ratio firstly drop slightly and then increases to approximately 100 vol% at point d′ (homogenization by inversion). However, a tiny amount of halite is produced at point d′ and total homogenization occurs at point d. Therefore, some underestimation of the homogenization temperature is inevitable in the microthermometric study of such fluid inclusions because the trace amount of halite cannot be observed. Continuous heating will follow the isochore d-j into the single-phase region (Fig. 1).

One more stage of evolution may occur if low-salinity fluid is trapped

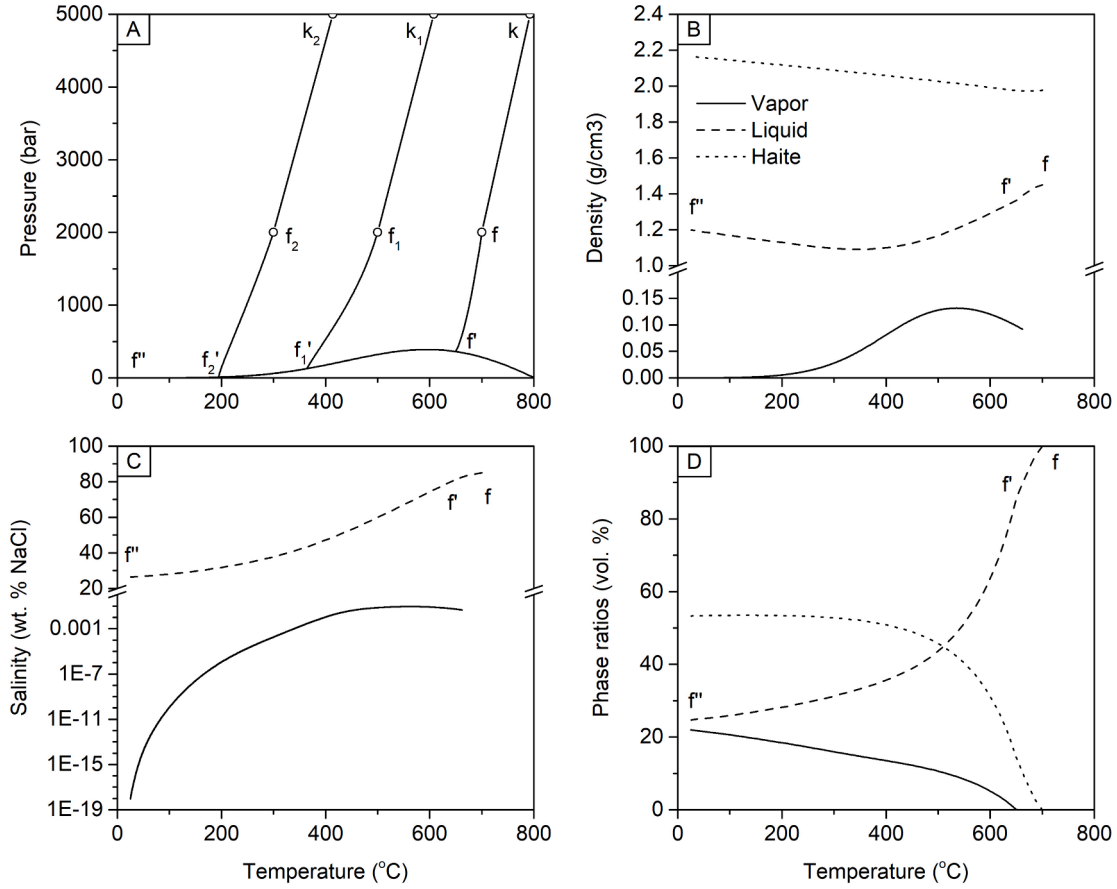

Fig. 16. Variations of fluid density, salinity, and fluid inclusion phase ratios with temperature for point f on the halite liquidus.

in the single-phase region at elevated temperature and low pressure (point j_0 in Fig. 18), so that the evolution may have two intersections with the bubble curve of the V + L + H surface (e.g., points d_1 and d_2 in Fig. 18). Evolution of the entrapped fluid at point j_0 (1000 ℃, 330 bar, 0.1 wt% NaCl) will intersect the bubble curve of the V + L region at point d_0 (900 ℃, 300 bar, 0.1 wt% NaCl). The following evolution is in the V + L region from d_0 to d_1 (718 ℃, 245 bar), in the V + H region from d_1 to d_2 (361 ℃, 123 bar), and in the V + L region from d_2 to d''. At point d_0, a tiny amount of high salinity fluid (93.2 wt% NaCl) is condensed in the fluid inclusion. At point d_1, the vapor and liquid phases in the fluid inclusion intersect the vapor and dew curves of the V + L + H surface, respectively. Upon leaving point d_1, the liquid phase is consumed and the halite phase emerges. Thereafter, it has the similar evolutionary path to d-d′-d″. The low volume ratios of halite and liquid at temperature above point d_2 are too small to be observed during microthermometric study. Therefore, such fluid inclusions, typically formed in very shallow porphyry systems (e.g., Muntean and Einaudi, 2000; Kodera et al., 2014; Mernagh and Mavrogenes, 2019), provides invalid temperature information for fluid evolution.

5. Implications

We systematically constructed the evolutionary paths for nine types of fluid inclusions trapped in variable conditions in the H_2O-NaCl system. These evolutionary paths are comprehensively illustrated in a pressure–temperature-salinity frame and a series of 2D figures to demonstrate the detailed evolution of salinity, density, and volume ratios of all the phases in fluid inclusions.

(1) Entrapment of an extremely low-salinity solution in the single-phase region will follow the isochores and intersect the bubble curve of the V + H region. The successive evolution will intersect the bubble curve of the V + L + H surface and then enter the V + L region to form a V + L type fluid inclusion. Upon heating, such a fluid inclusion will experience partial homogenization by the disappearance of liquid and appearance of trace amount of halite upon touching the V + L + H surface, followed by total homogenization by the disappearance of halite. Volume of the halite is too small to be observed, so the liquid disappearance temperature may be taken for the total homogenization temperature, leading to significant underestimation of temperature and pressure for the shallow magmatic-hydrothermal deposits.

(2) When isochores of a V + L type fluid inclusion intersect the V + L surface on the bubble curve, a high-density and high-salinity liquid phase will be condensed. The salinity of the liquid phase will approach the bulk salinity because the majority of the H_2O and NaCl is converted into the liquid phase. Homogenization by inversion is typical for such fluid inclusions, followed by a sharp increase of vapor ratio above the critical point of pure water. After that, the decrease of the vapor volume reaches a plateau stage with little volume change. The last droplet of liquid may persist for over two hundred degrees Celsius upon heating. Such a homogenization behavior is very likely to lead to the underestimation of homogenization temperature and pressure during microthermometric analysis.

(3) When an isochore of the entrapped fluid intersects the bubble curve at >696 ℃, it will evolve to be a V + L + H type fluid inclusion. Upon heating, such a fluid inclusion will experience partial homogenization by halite dissolution and total homogenization by liquid

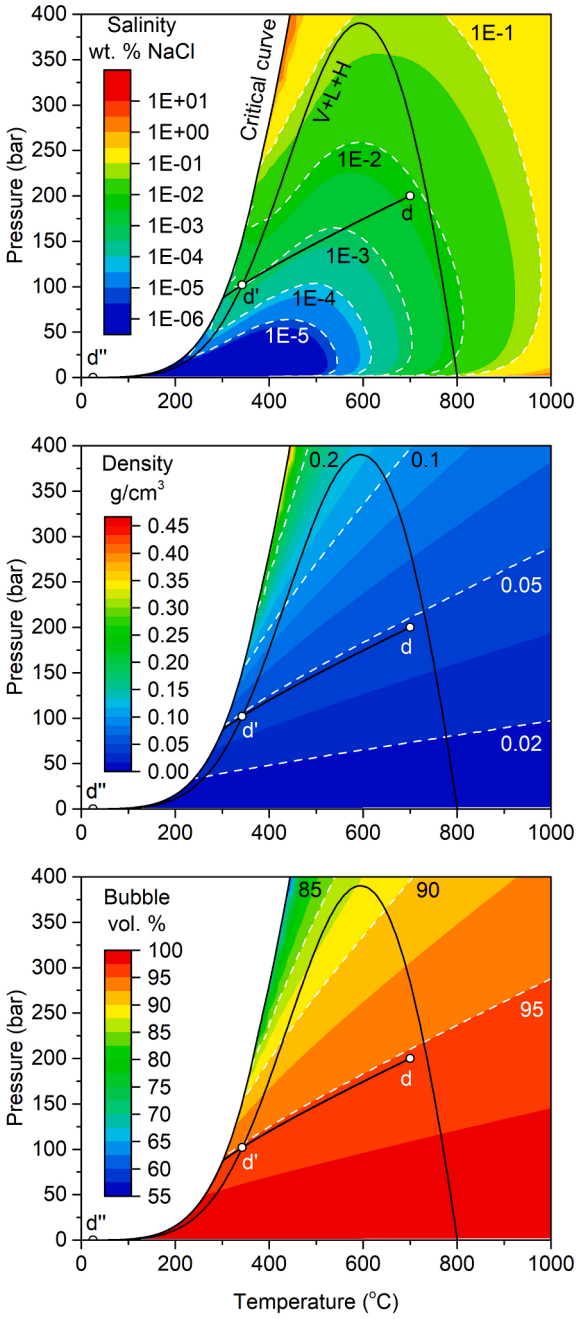

Fig. 17. Contour figures for the fluid salinity, density, and room-temperature phase ratios of corresponding fluid inclusions on the bubble curve of the V + H region. Evolution d-d′-d″ is consistent with that in Fig. 1.

disappearance.

(4) When isochores of a V + L or V + L + H type fluid inclusion intersect the V + L surface on the dew curve, a low-density and low-salinity vapor phase will be separated. The internal pressure of the vapor and liquid phases during evolution along the V + L surface is consistently lower than the pressure of the *iso*-salinity line at bulk salinity, because H_2O and NaCl are redistributed to form a vapor phase with lower salinity and a liquid phase with higher salinity.

(5) The residual vapor phase at halite dissolution for halite-bearing fluid inclusions may lead to an over-estimation of the bulk fluid salinity by over 3 % at elevated temperature conditions. Therefore, a correction is necessary especially for high-temperature fluid inclusions with a bulk salinity of around 50 wt% NaCl.

(6) Halite-saturated solutions at a given pressure produce fluid inclusions with larger volumes of halite when trapped at low temperature conditions compare to inclusions trapped at high temperature conditions. Therefore, the larger volume ratio of halite may suggest lower entrapment temperature or higher entrapment pressure instead of higher bulk salinity in halite-bearing fluid inclusions.

(7) The isochores on the halite liquidus display an anticlinal shape,

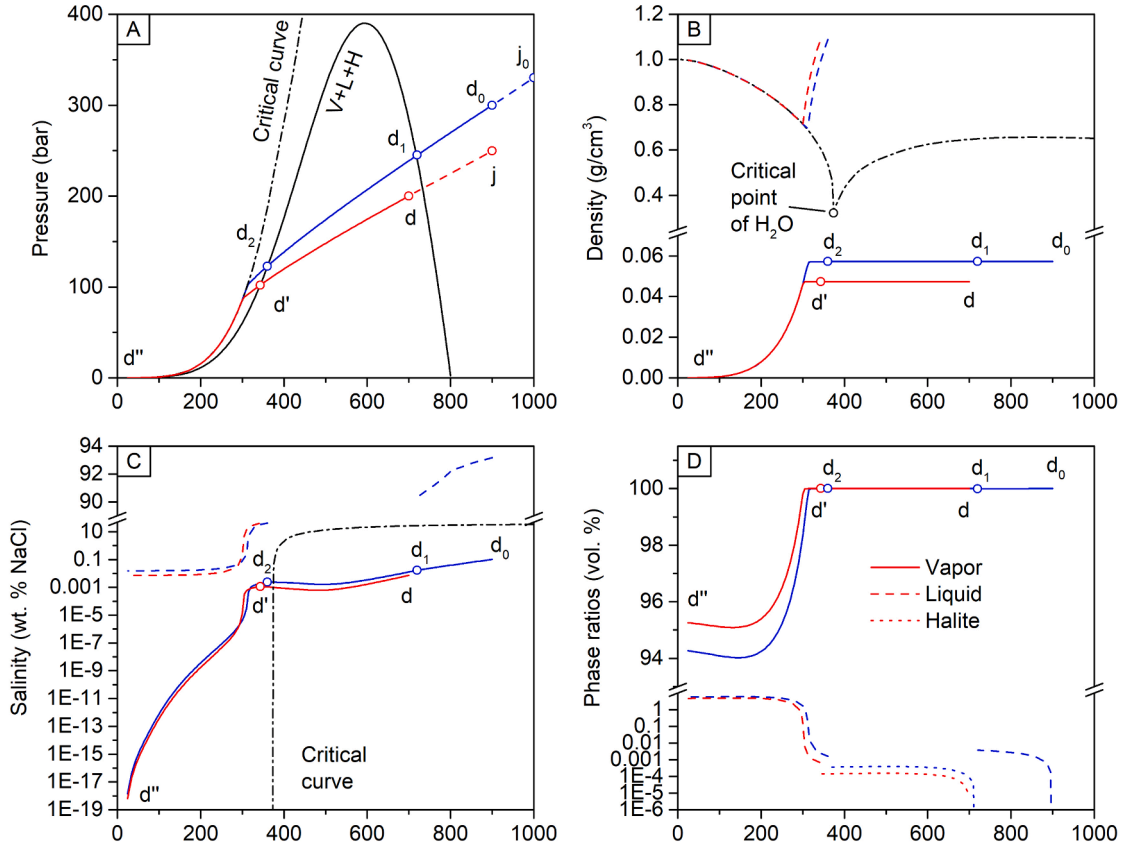

Fig. 18. Variations of fluid density, salinity, and fluid inclusion phase ratios with temperature for point d on the bubble curve of the V + H region.

Table 2
Tabulated data for the correction of salinity overestimation by halite dissolution temperature.

	Salinity													
Temperature	30	35	40	45	50	55	60	65	70	75	80	85	90	95
1000	0.1	0.4	0.9	1.5	1.8	1.9	1.8	1.7	1.6	1.4	1.2	0.9	0.6	0.3
950	0.1	0.4	0.9	1.4	1.7	1.8	1.7	1.7	1.5	1.3	1.0	0.8	0.5	0.2
900	0.1	0.3	0.8	1.3	1.6	1.7	1.7	1.6	1.4	1.2	0.9	0.6	0.4	0.2
850	0.0	0.3	0.8	1.2	1.5	1.6	1.6	1.5	1.3	1.0	0.8	0.5	0.3	0.1
800	0.0	0.3	0.7	1.1	1.4	1.5	1.5	1.3	1.1	0.9	0.6	0.4	0.2	0.0
750	0.0	0.3	0.7	1.1	1.3	1.4	1.4	1.2	1.0	0.7	0.5	0.2	0.1	
700	0.0	0.3	0.6	1.0	1.2	1.3	1.2	1.0	0.7	0.5	0.2	0.1		
650	0.0	0.3	0.6	0.9	1.0	1.0	0.9	0.7	0.5	0.2	0.0			
600	0.0	0.2	0.5	0.7	0.8	0.8	0.6	0.4	0.2					
550	0.0	0.2	0.4	0.6	0.6	0.5	0.3	0.1						
500	0.0	0.2	0.3	0.4	0.4	0.2	0.0							
450	0.0	0.1	0.2	0.2	0.1									
400	0.0	0.1	0.1	0.1										

Note: The top row is the bulk fluid salinity (wt. % NaCl). The first column is the entrapment temperature (°C).

because the increased salinity dominates the density on the halite liquidus at high temperature and reverses the slopes of the isochores. The pressure–temperature projections of the evolutionary paths along the halite liquidus shows notable curvature, because of the change of fluid density and salinity.

(8) The contour figures can facilitate the understanding of post-entrapment shrinkage or expansion of fluid inclusions which alters fluid inclusion phase ratios and homogenization behavior.

Although the H_2O-NaCl system is the most widely used binary system in the study of hydrothermal fluids in various geological settings, appreciable concentrations of other components, including KCl, $CaCl_2$, $FeCl_2$, and CO_2 etc., have been identified by quantitative compositional analyses (e.g., Heinrich et al., 1999; Audétat et al., 2008; Audétat, 2019). These additional components may notably alter the phase boundaries and fluid inclusion microthermometry behavior. For example, the univariant coexistence of Vapor + Liquid + Halite in the H_2O-NaCl system is increased to divariant with the addition of KCl (Lecumberri-Sanchez et al., 2020). Multiple daughter minerals with variable melting temperatures occur for more complicated systems (Steele-MacInnis et al., 2016). The readers are recommended to find more details for ternary systems H_2O-NaCl-KCl (e.g., Hall et al., 1988; Bodnar et al., 1989; Lecumberri-Sanchez et al., 2020), H_2O-NaCl-$CaCl_2$

(e.g., Vanko et al., 1988; Steele-MacInnis et al., 2011), H_2O-NaCl-$FeCl_2$ (e.g., Lecumberri-Sanchez et al., 2015a; Lecumberri-Sanchez et al., 2015b); and H_2O-NaCl-CO_2 (e.g., Brown and Lamb, 1989; Duan et al., 1995; Schmidt and Bodnar, 2000; Steele-MacInnis, 2018) where more complicated microthermometry behavior of fluid inclusions can be addressed.

Declaration of Competing Interest

The authors declare that they have no known competing financial interests or personal relationships that could have appeared to influence the work reported in this paper.

Data availability

Data will be made available on request.

Acknowledgements

We acknowledge our thanks to the editor Huayong Chen for handling this manuscript and to Robert Bodnar and Alexandre Tarantola for their constructive comments. This work was financially supported by the National Natural Science Foundation of China (NO. 42073045, 42121003), the Youth Innovation Promotion Association of the Chinese Academy of Sciences (NO. 2023416), the K.C. Wong Education Foundation (NO. GJTD-2020-13), a special fund managed by the State Key Laboratory of Ore Deposit Geochemistry, Chinese Academy of Sciences, and the Guizhou Provincial 2020 Science and Technology Subsidies (No. GZ2020SIG).

Appendix A. Supplementary data

Pressure, temperature, salinity, density, and volume ratios for each phase along the evolutionary paths for nine types of fluid inclusions in the H_2O-NaCl system. Supplementary data to this article can be found online at https://doi.org/10.1016/j.oregeorev.2023.105561.

References

Audétat, A., 2019. The metal content of magmatic-hydrothermal fluids and its relationship to mineralization potential. Econ. Geol. 114 (6), 1033–1056.
Audétat, A., Günther, D., Heinrich, C.A., 1998. Formation of a magmatic-hydrothermal ore deposit: insights with LA-ICP-MS analysis of fluid inclusions. Science 279 (5359), 2091–2094.
Audétat, A., Günther, D., 1999. Mobility and H_2O loss from fluid inclusions in natural quartz crystals. Contrib. Miner. Petrol. 137 (1–2), 1–14.
Audétat, A., Li, W.T., 2017. The genesis of Climax-type porphyry Mo deposits: Insights from fluid inclusions and melt inclusions. Ore Geol. Rev. 88, 436–460.
Audétat, A., Pettke, T., Heinrich, C.A., Bodnar, R.J., 2008. Special Paper: The composition of magmatic-hydrothermal fluids in barren and mineralized intrusions. Econ. Geol. 103 (5), 877–908.
Audétat, A., 2023. A Plea for More Skepticism toward fluid inclusions: Part II. Homogenization via halite dissolution in brine inclusions from magmatic-hydrothermal systems is commonly the result of postentrapment modifications. Econ. Geol., 118(1), 43–55.
Bakker, R.J., 2018. AqSo_NaCl: computer program to calculate p-T-V-x properties in the H_2O-NaCl fluid system applied to fluid inclusion research and pore fluid calculation. Comput. Geosci. 115, 122–133.
Bakker, R.J., 2019. Package fluids. Part 5: The NaCl-H_2O system in fluid inclusion research and applications of the software AqSo_NaCl (Bakker, 2018). Chem. Geol. 525, 400–413.
Bakker, R.J., Jansen, J.B.H., 1990. Preferential water leakage from fluid inclusions by means of mobile dislocations. Nature 345 (6270), 58–60.
Becker, S.P., Fall, A., Bodnar, R.J., 2008. Synthetic fluid inclusions. XVII.1 PVTX properties of high salinity H_2O-NaCl solutions (>30 wt % NaCl): application to fluid inclusions that homogenize by halite disappearance from porphyry copper and other hydrothermal ore deposits. Econ. Geol. 103, 539–554.
Becker, S.P., Bodnar, R.J., Reynolds, T.J., 2019. Temporal and spatial variations in characteristics of fluid inclusions in epizonal magmatic-hydrothermal systems: Applications in exploration for porphyry copper deposits. J. Geochem. Explor. 204, 240–255.
Bodnar, R.J., 1983. A method of calculating fluid inclusion volumes based on vapor bubble diameters and P-V-T-X properties of inclusion fluids. Econ. Geol. 78 (3), 535–542.
Bodnar, R.J., 1989. Synthetic fluid inclusions: A novel technique for experimental water-rock studies. In: Proceedings of the 6th International Water-Rock Symposium, pp. 99–102.
Bodnar, R.J., 1994. Synthetic fluid inclusions: XII. The system H_2O–NaCl. Experimental determination of the halite liquidus and isochores for a 40 wt% NaCl solution. Geochim. Cosmochim. Acta 58 (3), 1053–1063.
Bodnar, R.J., 2003. Interpretation of data from aqueous-electrolyte fluid inclusions. In: Samson, I.M., Anderson, A., Marshall, D. (Eds.), Fluid Inclusions: Analysis and Interpretation. Short Course Series Volume32. Mineralogical Association of Canada, Ottawa, pp. 81–100.
Bodnar, R.J., Sterner, S.M., Hall, D.L., 1989. SALTY: A FORTRAN program to calculate compositions of fluid inclusions in the system NaCl-KCl-H_2O. Comput. Geosci. 15 (1), 19–41.
Bodnar, R.J., Lecumberri-Sanchez, P., Moncada, D., Steele-MacInnis, M., 2014. Fluid inclusions in hydrothermal ore deposits. In: Turekian, K.K. (Ed.), Treatise on Geochemistry. Elsevier, Oxford, pp. 119–142.
Bodnar, R.J., Vityk, M.O., 1994. Interpretation of microthermometric data for H_2O-NaCl fluid inclusions. Fluid Inclus. Minerals, Methods Appl. 117–130.
Brown, P.E., Lamb, W.M., 1989. P-T-V properties of fluids in the system H_2O ±CO_2±NaCl: New graphical presentations and implications for fluid inclusion studies. Geochim. Cosmochim. Acta 53, 1209–1221.
Cline, J.S., Bodnar, R.J., 1991. Can economic porphyry copper mineralization be generated by a typical calc-alkaline melt? J. Geophys. Res. 96 (B5), 8113–12126.
Driesner, T., Heinrich, C.A., 2007. The system H_2O–NaCl. Part I: Correlation formulae for phase relations in temperature–pressure–composition space from 0 to 1000°C, 0 to 5000bar, and 0 to 1 XNaCl. Geochim. Cosmochim. Acta 71 (20), 4880–4901.
Duan, Z.H., Moller, N., Weare, J.H., 1995. Equation of state for the NaCl-H_2O-CO_2 System - prediction of phase-equilibria and volumetric properties. Geochim. Cosmochim. Acta 59 (14), 2869–2882.
Ermakov, N.P., 1965. Research on the Nature of Mineral-Forming Solutions. Pergamon Press, Oxford.
Hall, D.L., Sterner, S.M., Bodnar, R.J., 1988. Freezing point depression of NaCl-KCl-H_2O solutions. Econ. Geol. 83, 197–202.
Heinrich, C.A., Candela, P.A., 2014. Fluids and ore formation in the Earth's crust. Treatise Geochem. 13, 1–28.
Heinrich, C.A., Gunther, D., Audetat, A., Ulrich, T., Frischknecht, R., 1999. Metal fractionation between magmatic brine and vapor, determined by microanalysis of fluid inclusions. Geology 27 (8), 755–758.
Klyukin, Y.I., Steele-MacInnis, M., Lecumberri-Sanchez, P., Bodnar, R.J., 2019. Fluid inclusion phase ratios, compositions and densities from ambient temperature to homogenization, based on PVTX properties of H_2O H_2O-NaCl. Earth Sci. Rev. 198, 102924.
Knight, C.L., Bodnar, R.J., 1989. Synthetic fluid inclusions: IX. Critical PVTX properties of NaCl-H_2O solutions. Geochim. Cosmochim. Acta 53 (1), 3–8.
Kodera, P., Heinrich, C.A., Waller, M., Lexa, J., 2014. Magmatic salt melt and vapor: extreme fluids forming porphyry gold deposits in shallow subvolcanic settings. Geology 42 (6), 495–498.
Lecumberri-Sanchez, P., Steele-MacInnis, M., Bodnar, R.J., 2012. A numerical model to estimate trapping conditions of fluid inclusions that homogenize by halite disappearance. Geochim. Cosmochim. Acta 92, 14–22.
Lecumberri-Sanchez, P., Steele-MacInnis, M., Bodnar, R.J., 2015a. Synthetic fluid inclusions XIX. Experimental determination of the vapor-saturated liquidus of the system H_2O-NaCl-$FeCl_2$. Geochim. Cosmochim. Acta 148, 34–49.
Lecumberri-Sanchez, P., Steele-MacInnis, M., Weis, P., Driesner, T., Bodnar, R.J., 2015b. Salt precipitation in magmatic-hydrothermal systems associated with upper crustal plutons. Geology 43 (12), 1063–1066.
Lecumberri-Sanchez, P., Luo, M., Steele-MacInnis, M., Runyon, S.E., Matthew Sublett, D., Klyukin, Y.I., Bodnar, R.J., 2020. Synthetic fluid inclusions XXII: Properties of H_2O-NaCl ± KCl fluid inclusions trapped under vapor- and salt-saturated conditions with emphasis on the effect of KCl on phase equilibria. Geochim. Cosmochim. Acta 272, 78–92.
Lerchbaumer, L., Audétat, A., 2012. High Cu concentrations in vapor-type fluid inclusions: An artifact? Geochim. Cosmochim. Acta 88, 255–274.
Li, L., Ni, P., Wang, G.G., Zhu, A.D., Pan, J.Y., Chen, H., Huang, B., Yuan, H.X., Wang, Z. K., Fang, M.H., 2017. Multi-stage fluid boiling and formation of the giant Fujiawu porphyry Cu–Mo deposit in South China. Ore Geol. Rev. 81, 898–911.
Mao, W., Rusk, B., Yang, F., Zhang, M., 2017. Physical and chemical evolution of the Dabaoshan porphyry Mo deposit, South China: insights from fluid inclusions, cathodoluminescence, and trace elements in quartz. Econ. Geol. 112 (4), 889–918.
Mernagh, T.P., Mavrogenes, J., 2019. Significance of high temperature fluids and melts in the Grasberg porphyry copper-gold deposit. Chem. Geol. 508, 210–224.
Muntean, J.L., Einaudi, M.T., 2000. Porphyry gold deposits of the Refugio district, Maricunga belt, northern Chile. Econ. Geol. 95 (7), 1445–1472.
Roedder, E., 1971. Fluid inclusion studies on the porphyry-type ore deposits at Bingham, Utah, Butte, Montana, and Climax, Colorado. Econ. Geol. 66, 98–120.
Roedder, E., Bodnar, R.J., 1980. Geologic pressure determinations from fluid inclusion studies. Annu. Rev. Earth Planet. Sci. 8 (1), 263–301.
Rusk, B.G., Reed, M.H., Dilles, J.H., 2008. Fluid inclusion evidence for magmatic-hydrothermal fluid evolution in the porphyry copper-molybdenum deposit at Butte, Montana. Econ. Geol. 103 (2), 307–334.
Schmidt, C., Bodnar, R.J., 2000. Synthetic fluid inclusions: XVI. PVTX properties in the system H_2O-NaCl-CO_2 at elevated temperatures, pressures, and salinities. Geochim. Cosmochim. Acta 64 (22), 3853–3869.
Sourirajan, S., Kennedy, G.C., 1962. The system H_2O-NaCl at elevated temperature and pressures. Am. J. Sci. 260, 115–141.

Steele-MacInnis, M., 2018. Fluid inclusions in the system H_2O-NaCl-CO_2: An algorithm to determine composition, density and isochore. Chem. Geol. 498, 31–44.
Steele-MacInnis, M., Bodnar, R.J., Naden, J., 2011. Numerical model to determine the composition of H_2O–NaCl–$CaCl_2$ fluid inclusions based on microthermometric and microanalytical data. Geochim. Cosmochim. Acta 75 (1), 21–40.
Steele-MacInnis, M., Bodnar, R.J., 2013. Effect of the vapor phase on the salinity of halite-bearing aqueous fluid inclusions estimated from the halite dissolution temperature. Geochim. Cosmochim. Acta 115, 205–216.
Steele-MacInnis, M., Han, L., Lowell, R., Rimstidt, J., Bodnar, R., 2012a. Quartz precipitation and fluid inclusion characteristics in sub-seafloor hydrothermal systems associated with volcanogenic massive sulfide deposits. Central Eur. J. Geosci. 4 (2), 275–286.
Steele-MacInnis, M., Lecumberri-Sanchez, P., Bodnar, R.J., 2012b. HokieFlincs_H_2O-NaCl : A Microsoft Excel spreadsheet for interpreting microthermometric data from fluid inclusions based on the PVTX properties of H_2O-NaCl. Comput. Geosci. 49, 334–337.
Steele-MacInnis, M., Ridley, J., Lecumberri-Sanchez, P., Schlegel, T.U., Heinrich, C.A., 2016. Application of low-temperature microthermometric data for interpreting multicomponent fluid inclusion compositions. Earth Sci. Rev. 159, 14–35.
Sterner, S.M., Hall, D.L., Bodnar, R.J., 1988. Synthetic fluid inclusions. V. Solubility relations in the system NaCl-KCl-H_2O under vapor-saturated conditions. Geochim. Cosmochim. Acta 52 (5), 989–1005.
Tarantola, A., Diamond, L.W., Stünitz, H., 2010. Modification of fluid inclusions in quartz by deviatoric stress I: experimentally induced changes in inclusion shapes and microstructures. Contrib. Miner. Petrol. 160 (6), 825–843.
Tarantola, A., Diamond, L.W., Stünitz, H., Thust, A., Pec, M., 2012. Modification of fluid inclusions in quartz by deviatoric stress. III: Influence of principal stresses on inclusion density and orientation. Contrib. Miner. Petrol. 164 (3), 537–550.
Tattitch, B.C., Blundy, J.D., 2017. Cu-Mo partitioning between felsic melts and saline-aqueous fluids as a function of XNaCleq, fO_2, and fS_2. Am. Mineral. 102 (10), 1987–2006.
Ulrich, T., Gunther, D., Heinrich, C.A., 2001. The evolution of a porphyry Cu-Au deposit, based on LA-ICP-MS analysis of fluid inclusions: Bajo de la Alumbrera, Argentina. Econ. Geol. 96 (8), 1743–1774.
Vanko, D.A., Bodnar, R.J., Sterner, S.M., 1988. Synthetic fluid inclusions: VIII. Vapor-saturated halite solubility in part of the system NaCl-$CaCl_2$-H_2O, with application to fluid inclusions from oceanic hydrothermal systems. Geochim. Cosmochim. Acta 52 (10), 2451–2456.
Weis, P., Driesner, T., Heinrich, C.A., 2012. Porphyry-copper ore shells form at stable pressure-temperature fronts within dynamic fluid plumes. Science 338 (6114), 1613–1616.
Weis, P., Driesner, T., Coumou, D., Geiger, S., 2014. Hydrothermal, multiphase convection of H2O-NaCl fluids from ambient to magmatic temperatures: a new numerical scheme and benchmarks for code comparison. Geofluids 14 (3), 347–371.
Wilkinson, J.J., 2001. Fluid inclusions in hydrothermal ore deposits. Lithos 55 (1–4), 229–272.
Yardley, B.W.D., Bodnar, R.J., 2014. Fluids in the Continental Crust. GeochemPersp 3 (1), 1–127.
Zaheri-Abdehvand, N., Tarantola, A., Rasa, I., Hassanpour, S., Peiffert, C., 2020. Metal content and P-T evolution of CO_2-bearing ore-forming fluids of the Haftcheshmeh Cu-Mo porphyry deposit, NW Iran. J. Asian Earth Sci. 190, 104166.
Zhang, D., Audétat, A., 2023. A plea for more skepticism toward fluid inclusions: Part I. Postentrapment changes in fluid density and fluid salinity are very common. Econ. Geol., 118 (1), 15-41.